JEM Journal of Experimental Medicine

ARTICLE

Repertoire, function, and structure of serological antibodies induced by the R21/Matrix-M malaria vaccine

Jonathan R. McDaniel[1*], William N. Voss[1*], Georgina Bowyer[2], Scott A. Rush[1], Alexandra J. Spencer[2], Duncan Bellamy[2], Marta Ulaszewska[2], Jule Goike[1], Scott Gregory[3], C. Richter King[3], Jason S. McLellan[1], Adrian V.S. Hill[2], George Georgiou[1], Katie J. Ewer[2], and Gregory C. Ippolito[4]

The World Health Organization (WHO) recently recommended the programmatic use of the R21/Matrix-M vaccine for *Plasmodium falciparum* malaria prevention in children living in malaria-endemic areas. To determine its effects on humoral immunity, we conducted a proteomic analysis of polyclonal IgG antibodies directed against the NANP tetrapeptide of the circumsporozoite protein (CSP), which comprises the vaccine's core immunogen. In 10 malaria-naïve adult volunteers, R21/Matrix-M induced polarized IgG anti-NANP repertoires, heavily skewed for *IGHV3-30/3-33* genes bearing minimal somatic mutation, which remained static in composition following a controlled human malaria infection challenge. Notably, these vaccine-generated antibodies cross-reacted with another protective CSP epitope, the N-terminal junction region, despite its absence from the R21 construct. NANP-specific *IGHV3-30/3-33* mAbs mined from polyclonal IgG repertoires blocked sporozoite invasion in vitro and prevented parasitemia in vivo. Overall, R21/Matrix-M elicits polarized, minimally mutated, polyclonal IgG responses that can target multiple protective CSP epitopes, offering molecular insight into the serological basis for its demonstrated efficacy against *P. falciparum* malaria.

Introduction

Plasmodium falciparum (Pf) malaria is one of the world's most ancient diseases and remains the deadliest parasitic disease worldwide. The World Health Organization (WHO) estimated there were ∼608,000 malaria-related deaths worldwide in 2022 (Venkatesan, 2024). Although there are vaccine candidates under development that target each stage of the parasite's life cycle, vaccines targeting the pre-erythrocytic malarial sporozoite phase are the most advanced. This malaria vaccine approach remains an area of intense research due to its potential to entirely circumvent liver and blood-stage infection and thereby prevent disease and onward transmission.

The circumsporozoite protein (CSP), the primary outer coating essential for sporozoite development and hepatocyte invasion, has long been an attractive malaria vaccine target as it is highly immunogenic and capable of inducing a dominant neutralizing titer after infection or vaccination (Hill, 2006; Kappe et al., 2004; Nussenzweig and Nussenzweig, 1989). Earlier in vitro studies have demonstrated antibodies targeting CSP can prevent sporozoites from infecting liver cells (Hollingdale et al., 1984). In murine models, both passive transfer of polyclonal and mAbs against the immunodominant B cell major repeat epitope of CSP and active immunization with constructs containing this epitope confer protection against sporozoite challenge (Foquet et al., 2014; Oyen et al., 2017; Wang et al., 1995; Zavala and Chai, 1990).

Pf CSP (PfCSP) consists of three antigenic domains: an N-terminal junctional domain with a highly conserved pentapeptide sequence, an immunodominant central repeat region consisting of ∼45 tetrapeptides (NANP "major repeat" and NPDP and NVDP "minor repeats"), and concludes with a C-terminal domain. The Asn-Ala-Asn-Pro (NANP) tetrapeptide of the central repeat region constitutes the immunodominant B cell epitope of PfCSP (Dame et al., 1984; Zavala et al., 1983), and IgG1 and IgG3 constitute the majority of the anti-PfCSP serological response (Ubillos et al., 2018). After more than six decades of diligent effort to create an effective preerythrocytic malaria

[1]The University of Texas at Austin, Austin, TX, USA; [2]The Jenner Institute, University of Oxford, Oxford, UK; [3]Center for Vaccine Innovation and Access, PATH, Washington, DC, USA; [4]Texas Biomedical Research Institute, San Antonio, TX, USA.

*J.R. McDaniel and W.N. Voss contributed equally to this paper. Correspondence to Katie J. Ewer: katie.j.ewer@gsk.com; Gregory C. Ippolito: gippolito@txbiomed.org

A.J. Spencer's current affiliation is School of Biomedical Sciences and Pharmacy, University of Newcastle, Australia. J.R. McDaniel's current affiliation is Biomedicine Design, Pfizer, Cambridge, MA, USA. K.J. Ewer's current affiliation is GSK Vaccines Institute for Global Health (Global Health Vaccines R&D), GSK, Siena, Italy.

vaccine based on PfCSP, in the last three years, two have been recommended by WHO for use in children living in malaria-endemic areas: RTS,S/AS01 (brand name Mosquirix, by GlaxoSmithKline) and R21/Matrix-M (developed by the University of Oxford's Jenner Institute and manufactured by the Serum Institute of India).

RTS,S/AS01, recommended by WHO in 2021, is a chimera between the hepatitis B surface antigen and a truncated form of PfCSP that includes a portion of the unstructured and immunodominant NANP-repeating peptide and the C terminus domain (Miura et al., 2024; White et al., 2015; Zavala, 2022). Although several recent clinical trials have demonstrated RTS,S is safe and offers a high degree of protection immediately following vaccination, both the anti-CSP antibody titer and vaccine efficacy against infection wane over time (White et al., 2015; Zavala, 2022).

R21/Matrix-M was added to the WHO recommendation in October 2023 due to its demonstrated high efficacy (Datoo et al., 2024). The availability of R21/Matrix-M complements the ongoing distribution of RTS,S (Nnaji et al., 2024; Schmit et al., 2024) and greatly enhances overall access to malaria vaccines. R21/Matrix-M is a virus-like particle vaccine that targets the same CSP antigen as RTS,S and consists of Pf strain NF54, containing 19 copies of the NANP central repeat, and is formulated with Matrix-M adjuvant. Clinical trials of R21/Matrix-M have demonstrated high vaccine efficacy over one year with a three-dose regimen in 4,644 children aged 5–36 mo. Results indicate efficacy rates of 75% (95% confidence interval [CI] 71–79) at sites with moderate to high seasonal malaria transmission and 68% (95% CI 61–74) at sites with low to moderate perennial malaria transmission (Datoo et al., 2024). At this stage, trials of R21/Matrix-M have not been conducted in areas of high perennial transmission, and published trials do not yet allow for direct comparisons between the efficacy of the two vaccines (Moorthy et al., 2024). Mathematical modeling of three years of follow-up data stemming from an earlier phase 2b trial found that anti-CSP antibody titers satisfy the criteria for an immunological correlate of protection for R21/Matrix-M vaccine efficacy against clinical malaria (Schmit et al., 2024).

Whereas prior studies have examined the molecular features of anti-CSP antibody responses when elicited by natural infection, attenuated Pf whole-sporozoite (PfSPZ) vaccination, or RTS,S/AS01 vaccination, the molecular features of anti-CSP antibody responses following R21/Matrix-M vaccination have yet to be investigated. Until now, human CSP-reactive mAbs have been isolated exclusively by single-cell cloning using peripheral B cells (Imkeller et al., 2018; Kisalu et al., 2018; Murugan et al., 2018; Oyen et al., 2017; Tan et al., 2018; Triller et al., 2017; Williams et al., 2024). In these studies, B cells express germline antibodies or antibodies with low levels of mutation that preferentially express the highly homologous, allelically diverse *IGHV3-30* or *IGHV3-33* gene segments, which can mediate NANP recognition via a conserved tryptophan residue at position 52 (Trp52) of the germline-encoded complementarity determining region 2 of the heavy-chain variable region (CDR-H2) (Pholcharee et al., 2020). In contrast, the CSP epitopes targeted by the actual circulating plasma Igs (IgG) in vaccinated study subjects—especially those plasma antibodies that are most abundant and thereby play a dominant role in the polyclonal response—remain unknown.

Technological advances now provide a means to directly probe endogenous plasma IgG antibodies (de Graaf et al., 2022; Lavinder et al., 2015; Schulte et al., 2022; Townsend et al., 2024). Here, capitalizing on such advances, we set out to address at the molecular level the PfCSP humoral immune response induced by R21/Matrix-M vaccination in malaria-naïve volunteers, analyzing the plasma IgG antibody response to a $NANP_6$ peptide (NANP hexamer) after vaccination as well as before and after a controlled human malaria infection (CHMI) challenge. In this study, we show that the R21/Matrix-M malaria vaccine elicits a highly focused IgG humoral response in malaria-naïve individuals, predominantly involving minimally mutated antibodies utilizing *IGHV3-30/3-33* genes, consistent with previous observations of B cell responses. Our findings extend this understanding by demonstrating that the IgG response remains both stable in quantity and unaltered in its antibody composition, even following CHMI. Additionally, a key discovery is the cross-reactivity of these vaccine-induced IgG antibodies with the N-terminal junction of the CSP, an epitope not included in the R21 vaccine, indicating epitope spreading within the serological repertoire. Altogether, our data offer a molecular-level dissection of R21/Matrix-M IgG humoral immunity and provide a foundation to explain, in part, the demonstrated vaccine efficacy of R21/Matrix-M.

Results

Antibody lineage diversity in R21/Matrix-M–vaccinated individuals

A synergistic combination of Ig mass spectrometry (Ig-Seq) and B cell receptor (BCR) deep sequencing (BCR-Seq) was used to analyze the molecular composition and relative abundance of circulating anti-NANP IgG antibodies (see Materials and methods). For Ig-Seq proteomics, total IgG purified from volunteer plasma was subjected to affinity chromatography using recombinant NANP polypeptide (Asn-Ala-Asn-Pro hexamer [$NANP_6$]) representative of the CSP central repeat region. The eluted fraction ("$NANP_6$-reactive" IgG) and flow-through fraction ("$NANP_6$-nonreactive" IgG) were analyzed by high-resolution liquid chromatography and tandem mass spectrometry (LC–MS/MS). For BCR-Seq, next-generation sequencing (NGS) of peripheral blood BCR heavy-chain (VH), light-chain (VL), and single B cell–paired VH:VL variable region repertoires was performed. High-confidence IgG peptide spectral matches from the LC-MS/MS could then be identified using these volunteer-specific BCR databases—focusing on VH-derived hypervariable CDR-H3 peptides in particular—to determine the presence and relative abundance of IgG antibodies at both the lineage (family) and clonal (individual) levels. The integration of IgG peptide sequencing (Ig-Seq) with matching VH/VH:VL DNA sequencing (BCR-Seq) (Lavinder et al., 2015; Lavinder et al., 2014; Voss et al., 2021) allowed us to precisely identify and quantify circulating $NANP_6$-reactive IgG repertoires across a volunteer cohort at the molecular level. This approach also facilitated the cloning and

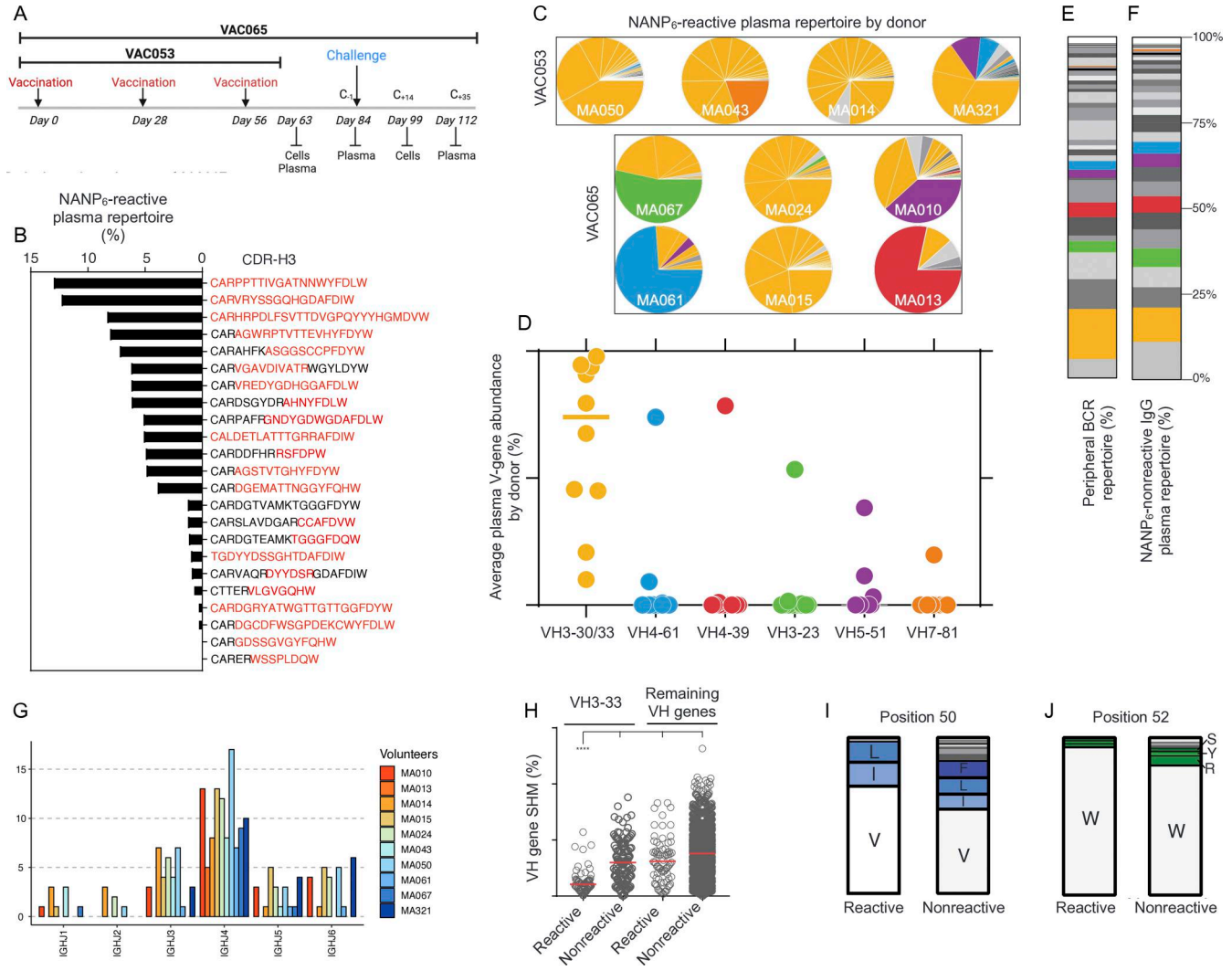

Figure 1. **Minimally mutated *IGHV3-30/3-33* genes dominate the IgG anti-NANP$_6$ plasma repertoire following three doses of R21/Matrix-M vaccine.** **(A)** Schematic of the VAC053 and VAC065 clinical trials. Plasma and cells (PBMCs) were collected at the times indicated. Volunteers (n = 10) were vaccinated at three time points (days 0, 28, and 56). Ig-Seq analyses were performed at day 63 (VAC053) or day 84 (VAC065). **(B)** Relative abundance of NANP$_6$-reactive IgG lineages in a representative volunteer. Each bar represents a single IgG lineage identified by its respective CDR-H3. Red indicates the unique peptides for each lineage that were detected by LC-MS/MS. **(C)** Relative plasma antibody IGHV gene segment usage for each volunteer. IGHV gene identity by color is shown in D. **(D)** Average IGHV gene abundance in NANP$_6$-reactive IgG. Bar represents mean. **(E)** IGHV gene frequency, by lineage, in total peripheral B cells averaged across all volunteers. **(F)** IGHV gene frequency, by lineage, in NANP$_6$-nonreactive IgG averaged across all volunteers. **(G)** IGHJ gene usage in the same volunteer as B. **(H)** IGHV gene SHM levels for NANP$_6$-reactive and nonreactive plasma IgG antibodies and BCR sequences grouped by lineage. ****P < 0.0001 (two-tailed Kruskal–Wallis test). **(I and J)** Amino acid usage in CDR-H2 (I) position 50 and (J) position 52 of *IGHV3-33* plasma antibodies separated by NANP$_6$ reactivity. I = isoleucine; L = leucine; V = valine; W = tryptophan. For each Ig-Seq analysis of polyclonal anti-NANP$_6$ IgG, the affinity purification was performed once, and the purified material was analyzed in triplicate by mass spectrometry.

validation of a small panel of recombinant IgG anti-NANP plasma mAbs for subsequent validation and functional assessment.

To evaluate the quality and evolution of the IgG humoral immune response to vaccination, we analyzed peripheral blood mononuclear cells (PBMC) and plasma samples collected from ten malaria-naïve volunteers in two separate phase I/IIa clinical trials, VAC053 (n = 4) and VAC065 (n = 6) (Fig. 1 A) (Venkatraman et al., 2025a; Venkatraman et al., 2025b; Venkatraman et al., 2024). In both trials, three intramuscular vaccinations were administered in 4-wk intervals on days 0, 28, and 56. For BCR-Seq, PBMC (containing antibody-secreting plasmablasts) were collected on day 63 from all 10 volunteers 1 wk after the third and final vaccination on day 56. For Ig-Seq, post-vaccination plasma was collected either on day 63 (VAC053) or on day 84 (VAC065). Unlike VAC053, volunteers in the VAC065 trial were challenged by CHMI with live sporozoite 4 wk after the day 56 final vaccination, with post-vaccination pre-challenge plasma collected on day 84 (referred to as "C$_{-1}$"). VAC065 volunteers were monitored for protection from infection until a final blood draw 5 wk later on day 112 (referred to as "C$_{+35}$"). Thus, plasma samples were analyzed after vaccination (VAC053 and VAC065) and after challenge (VAC065).

First, we set out to address fundamental questions about IgG repertoires generated by R21/Matrix-M vaccination: Are they

Table 1. **Summary of VAC053 and VAC065 clinical trials and the IgG humoral immune response to R21/Matrix-M vaccination**

Trial	Volunteer	Lineages (#)	IGHV3-30/33 (#)	IGHV3-30/33 relative abundance (%)	Titer (µg/ml)
VAC053	14	23	21	90.8	64.2
	43	16	13	79.5	10.0
	50	33	13	93.9	19.7
	321	23	7	67.6	7.3
VAC065	1010	24	12	45.6	63.1
	1024	27	20	94.5	53.0
	1067	11	6	44.9	38.6
	1013	5	1	10.0	40.0
	1015	28	24	97.8	43.5
	1061	10	7	20.7	45.6

Titers against $NANP_6$ peptide were measured by indirect ELISA at day 63 (VAC053) and day 84 (VAC065).

simple or complex in terms of the number of antibody lineages (i.e., families of closely related antibody VH sequences)? Is the distribution of lineages uniform or polarized? In our study the average IgG anti-$NANP_6$ titer among the 10 volunteers was 38.5 ± 20.3 µg/ml, as determined by ELISA (Table 1). This result indicated a substantial level of circulating IgG, which was sufficient for further analysis using $NANP_6$ affinity chromatography, and Ig-Seq proteomic deconvolution to identify and quantify IgG lineages. Because this was a "virgin" immune response in malaria-naïve volunteers, these IgG lineages likely derived from the activation of a single naïve B cell, which then clonally diversified through somatic hypermutation (SHM).

In one representative volunteer, the IgG anti-$NANP_6$ repertoire comprised 21 distinct antibody lineages, each exceeding a relative abundance threshold of >0.5% (Fig. 1 B). Similarly, the size of the IgG anti-$NANP_6$ repertoire was consistent across VAC053 and VAC065 volunteers, with an average of 20 ± 9 antibody lineages (range: 5–33) contributing to the $NANP_6$ reactivity (Fig. S1 A; and Tables 1 and S1), similar to other reports of antigen-specific serological repertoires analyzed through proteomic mass spectrometry (Bondt et al., 2021; Townsend et al., 2024). The serological IgG anti-NANP repertoires also displayed a significant degree of polarization; typically, the two to five most prevalent lineages, out of the ∼20 per volunteer, accounted for over 50% of the $NANP_6$ antigen-reactive titer (Fig. 1 C and Table S1).

Despite IgG repertoires being oligoclonal and polarized, the CDR-H3 region of antibody combining sites—a somatically generated, key determinant of binding specificity for most antibodies (Ippolito et al., 2006; Xu and Davis, 2000)—was diverse in both length (range: 6–26 aa) (Fig. S1 B) and sequence composition (Table S1). Among 197 total IgG lineages derived from the 10 volunteers, there was no CDR-H3 repertoire overlap, nor any apparent repertoire convergence among volunteers according to nonlinear dimensionality reduction (t-distributed stochastic neighbor embedding [tSNE]) analysis, and therefore no evidence for "public" multi-donor anti-$NANP_6$ antibodies (Fig. S1, C and D).

Dominant *IGHV3-30/3-33* gene usage in R21/Matrix-M–vaccinated individuals

Contrary to these features of diversity, a common characteristic across all the $NANP_6$-reactive IgG repertoires was an obvious enrichment for the variable-region gene segments *IGHV3-30*, *IGHV3-33*, or their related alleles (Fig. 1 D and Fig. S1 E). This VH family, including alleles with serine, arginine, or tryptophan at position 52 of the CDR-H2 (collectively referred to as "*IGHV3-30/33*"), encompasses *IGHV3-30*, *IGHV3-30-3*, *IGHV3-30-5*, and *IGHV3-33* alleles that share over 96% identity (Tan et al., 2018). On average, *IGHV3-30/33* circulating IgG antibodies constituted ∼70% of the $NANP_6$-reactive repertoire after vaccination (Fig. 1 D). Similarly, most PfCSP repeat mAbs isolated by single-cell cloning of peripheral human B cells are predominantly encoded by *IGHV3-30/33* (Julien and Wardemann, 2019). While other IGHV genes played dominant roles in certain individuals in both the VAC053 and the VAC065 cohorts (Fig. 1, C and D), their infrequent usage suggests volunteer-specific, nonpublic motifs. In four of six VAC065 volunteers, non-*IGHV3-30/33* genes increased in relative plasma abundance by day 84 after vaccination (MA010, MA013, MA061, and MA067); however, this was not the case for two of six VAC065 volunteers (MA015 and MA024), wherein *IGHV3-30/33* dominance continued to prevail. We then compared the total peripheral B cell IgG repertoire from NGS (Fig. 1 E) with the $NANP_6$-nonreactive plasma IgG repertoire (Fig. 1 F). Averaged over the 10 volunteers, the similarity in *IGHV3-30/33* frequency between the BCR-sequencing repertoire (14.7%) and the nonreactive plasma repertoire (10.1%) indicates that the observed ∼70% IGHV3-30/33 bias in the $NANP_6$-binding plasma IgG repertoire reported in Fig. 1 D must be due to antigen-specific enrichment. In contrast to the IGHV bias, IGHJ gene usage in plasma or the BCR repertoire was highly diversified and non-polarized (Fig. 1 G).

Another common characteristic of $NANP_6$-reactive plasma antibodies was a significant reduction in SHM among those using the *IGHV3-33* gene segment. Antibody lineages not using *IGHV3-33* showed SHM rates approximately threefold higher than those using *IGHV3-33* (6.2% ± 4.8 versus 2.1% ± 1.9; Fig. 1 H).

In support of the hypothesis that NANP recognition is fundamentally enhanced by amino acid encoded in the germline of the *IGHV3-33* gene segment (CDR-H2 Val50 and Trp52, in particular) (Wahl and Wardemann, 2022), it was found that $NANP_6$-nonreactive *IGHV3-33* antibodies were nearly three times more mutated compared with $NANP_6$-reactive antibodies (6.0% ± 3.8 versus 2.1% ± 1.9, respectively). Of note, nonreactive antibodies had a higher number of replacement mutations at positions Val50 and Trp52 (Fig. 1, I and J). Altogether, our results illustrate that the antibody features of the serological repertoire are consistent with findings from the analysis of IgG receptors isolated by B cell cloning showing that *IGHV3-30/33* genes (*IGHV3-33* primarily) confer binding to the CSP NANP major repeat without reliance on any exact CDR-H3 structure, IGHJ sequence, or acquired somatic mutations during B cell evolution.

Antibody lineage diversity in R21/Matrix-M–vaccinated individuals remains unchanged following sporozoite challenge

Mosquito bites delivering sporozoite-stage malaria parasites have traditionally served as a model for testing preerythrocytic stage vaccines. Here, to gain a deeper understanding of the stability and quality of IgG anti-NANP antibodies induced by R21/Matrix-M vaccination, *Anopheles stephensi* mosquitoes and the chloroquine-sensitive NF54 strain (3D7 clone) of Pf were used for CHMI. To evaluate the immune response to vaccination and sporozoite challenge, we analyzed the IgG repertoire after vaccination in $n = 5$ volunteers at day 84 (C_{-1}) and then monitored for protection from infection until a final blood draw 5 wk later at day 112 (C_{+35}). Fig. 2, A and B show plasma antibody repertoires induced by R21/Matrix-M vaccination remained stable despite challenge, with a protected (Fig. 2 A) and a non-protected (Fig. 2 B) volunteer displaying consistent IgG lineage composition and relative abundance profiles for their $NANP_6$-reactive repertoires. The high degree of correlation between pre- and post-challenge repertoires is shown in scatter plots representing the relative abundance of each identified lineage at the time of plasma collection. The relative abundance of detectable $NANP_6$-reactive IgG antibodies in protected volunteer MA-1010 (Fig. 2 A), for instance, was strikingly correlated lineage-for-lineage and nearly indistinguishable before and after challenge (Pearson correlation, $r^2 = 0.98$). In non-protected subject MA-1015, the pre- and post-challenge IgG repertoires were similarly highly correlated at $r^2 = 0.88$ (Fig. 2 B). A strong degree of correlation ($r^2 > 0.6$) held for all five volunteers (Fig. S2). 35 days, or approximately two IgG1 half-lives, separated the pre- and post-challenge time points, suggesting that the volunteers' static IgG repertoires are maintained by established, dynamic pools of antibody-secreting cells.

Given the static composition of IgG lineages before and after challenge with sporozoite, we wondered whether this molecular feature might also be reflected at the bulk serological level. Using a larger VAC065 cohort of 17 volunteers, we observed $NANP_6$ titers in both protected and non-protected groups showed no boosting effect after sporozoite challenge (Fig. 2, C and D). In fact, collectively, titers declined by an average of 27% between days C_{-1} and C_{+35} over the 5-wk period between challenge and plasma collection. No significant differences were observed before challenge or after challenge between the absolute (μg/ml) or the relative (%) changes in titer when comparing protected and non-protected individuals. Upon reexamination of the subset of five volunteers analyzed by Ig-Seq, we note that persistent antibodies, defined as those present before and after challenge, accounted for over 95% of the total $NANP_6$-reactive repertoire (Fig. 2 E), with <5% of plasma antibodies after challenge being detectable only at the second time point (Fig. 2 F), which could explain in part the static or else decreased titers measured by bulk serology.

Cross-reactive antibodies induced by R21/Matrix-M target multiple CSP epitopes PfCSP features a "junction region" (JR) that connects the N-terminal domain to the central NANP repeat region. In the Pf reference isolate 3D7 (PfCSP_3D7), the JR starts with the sequence NPDP, followed by three interspersed NANP and NVDP repeats, with NPDP being unique to this region. Studies have shown that mAbs targeting the JR epitope in both mice and humans can be protective (Kayentao et al., 2022; Kayentao et al., 2024; Wang et al., 2020). B cell repertoire analyses have identified antibodies specific to the NANP sequence, and those cross-reactive with the JR are encoded by *IGHV3-30/33* genes, particularly *IGHV3-33* paired with *IGKV1-5* (reviewed in Julien and Wardemann [2019]). In contrast, antibodies specific to the NVDP sequence and those cross-reactive with both NVDP and NPDP utilize various IGHV gene segments (Kisalu et al., 2018; Murugan et al., 2020). Notably, all JR-binding mAbs exhibit some level of cross-reactivity with NANP (Murugan et al., 2020). Despite the R21 vaccine containing only a truncated form of PfCSP with 19 NANP repeats and the C terminus—lacking the N terminus, as well as the NPDP and NVDP repeats of the JR (Collins et al., 2017; Stoute et al., 1997)—we found R21/Matrix-M could induce JR-reactive plasma antibodies in all five VAC065 volunteers tested at day 84 after vaccination (Fig. 3). The depletion of pre-challenge (C_{-1}) and post-challenge (C_{+35}) polyclonal IgG using $NANP_6$ affinity chromatography led to a significant reduction in JR-binding signals, as measured by indirect ELISA with a peptide encompassing the JR epitope (JR peptide: KQPADGNPDPNANPNVDPN).

To validate this at the molecular level, Ig-Seq analysis of pre-challenge IgG from one volunteer (MA-1010) using two separate pulldowns ($NANP_6$ and JR) demonstrated that the JR-reactive repertoire overlapped with the $NANP_6$-reactive repertoire lineage-for-lineage. Thus, in this volunteer, the JR-binding antibody lineages were a subset of the broader anti-$NANP_6$ repertoire. Of the seven JR cross-reactive lineages identified in MA-1010 (meeting quality criteria and exceeding 0.5% relative abundance), there was diverse IGHV gene usage, with only one lineage employing an *IGHV3-30/33* family member (VH3-30). These seven lineages exhibited minimal somatic mutation in their IGHV gene segments (average 2.6%). The predominant lineage (VH3-7 at 47.5% relative abundance) had merely a single Asn52 mutation in its CDR-H2. Asn52 was previously identified as a key interacting residue in the dual-reactive mAbs Ab668 and CIS42 targeting NANP/JR (Kisalu et al., 2018; Oyen et al., 2020).

Overall, these results suggest the NANP polypeptide of the central repeat region in the R21/Matrix-M vaccine is sufficient to instigate the generation and/or evolution of diverse,

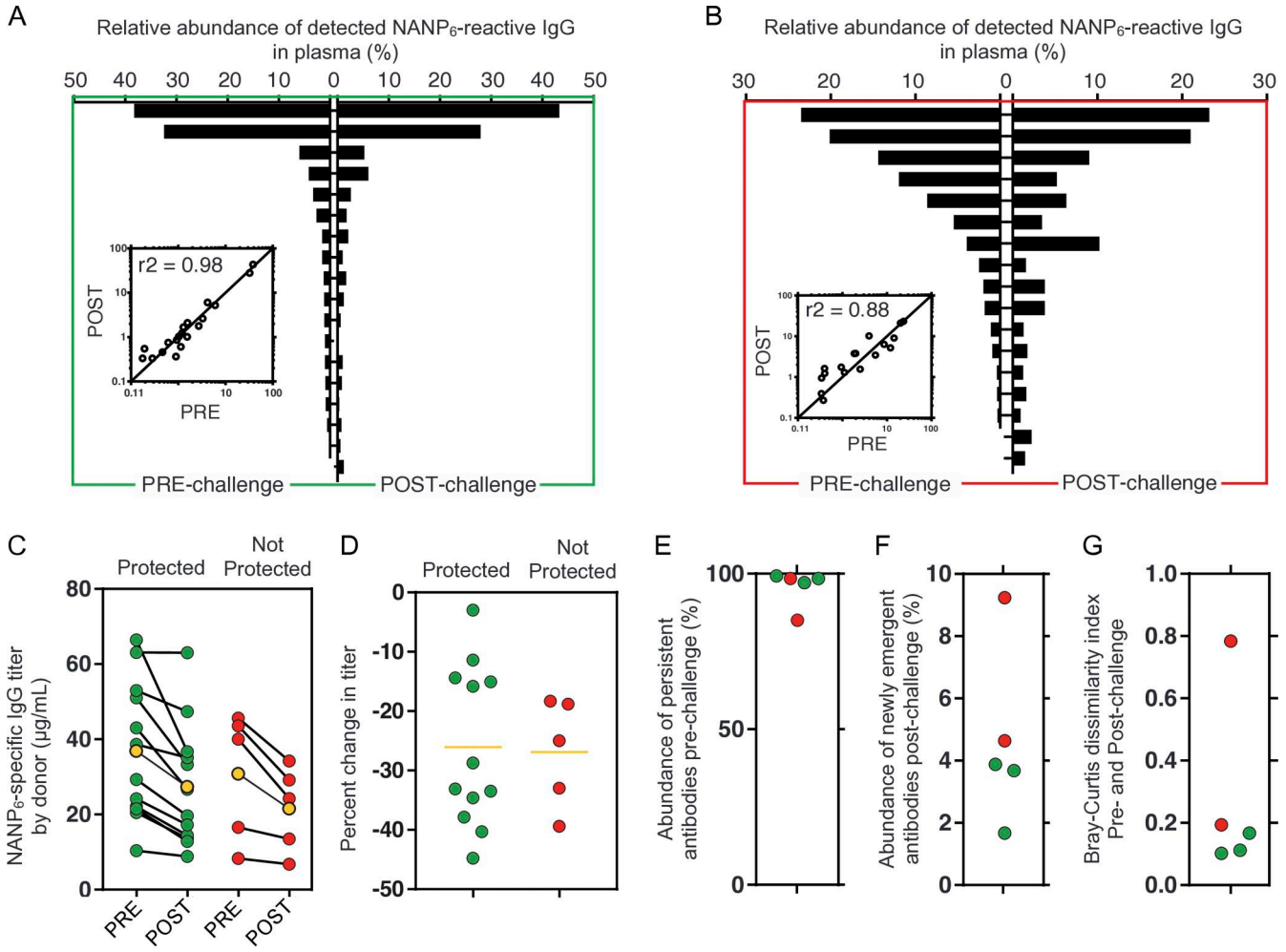

Figure 2. **Following vaccination with R21/Matrix M, $NANP_6$-reactive plasma antibody repertoires remain highly correlated before and after challenge with live sporozites.** A subset of thrice-vaccinated VAC065 volunteers (n = 5) was analyzed at day 84 (pre-challenge; C_{-1}) and 5 wk later at day 112 (post-challenge; C_{+35}). **(A and B)** Relative abundance of $NANP_6$ reactive IgG lineages before and after challenge for one representative protected individual (A) and one non-protected individual (B). Each bar represents one lineage. Inset indicates relative abundance for each lineage before and after challenge (Pearson r^2 = 0.98 [A] and r^2 = 0.88 [B]). **(C and D)** Estimated plasma titer (C) and (D) change in titer of $NANP_6$-reactive IgG for volunteers before and after challenge (n = 17). Yellow markers indicate the group average. **(E)** Abundance of persistent antibodies before challenge (n = 5). **(F)** Abundance of emergent antibodies after challenge (n = 5). **(G)** Bray–Curtis dissimilarity index between pre- and post-challenge repertoires (n = 5). Lower values indicate higher degrees of similarity. Green indicates protection from infection; red indicates no protection. For each Ig-Seq analysis of polyclonal anti-$NANP_6$ IgG, the affinity purification was performed once, and the purified material was analyzed in triplicate by mass spectrometry.

near-germline IgG antibodies that are cross-reactive with the N-terminal junction—even though the JR is absent from the vaccine construct.

R21/Matrix-M vaccine-induced *IGHV3* family antibodies show robust anti-sporozoite activity

From VAC053 immunized volunteers, a small panel of nine PfCSP plasma mAbs (VH:VL pairs) were isolated from day 63 (day 7 after third vaccination) peripheral blood B cells. These nine plasma mAbs mapped with high confidence to proteomic CDR-H3 peptides of $NANP_6$-reactive IgG lineages identified by Ig-Seq proteomic analysis (and circulating at >0.5% relative abundance). mAbs were expressed recombinantly as full-length IgG1 and first tested for $NANP_6$ peptide-binding specificity by ELISA. Anti-sporozoite binding and inhibitory activity were also initially evaluated and compared with two previously characterized mAbs derived from B cells of naturally exposed individuals in Africa (Triller et al., 2017); these two mAbs, 663 and 580, can inhibit Pf sporozoite traversal in hepatocytes in vitro and recognize transgenic *Plasmodium berghei* (Pb) parasites expressing PfCSP (PfCSP@PbCSP).

Three positive IgG plasma mAbs were prioritized for full, replicate downstream experimentation (Table 2). All three antibodies use *IGHV3-30/33* genes and represent a range of serological abundances, extremes of somatic mutation, and diverse expression of Ig light chains: MA1 (13% abundance; 1.6% SHM; *IGLV1-40*), MA6 (0.6%; 1.7%; *IGKV1-5*), and MA8 (19.6%; 8.2%; *IGKV1-16*). One negative *IGHV1-69* mAb (MA5) was also carried forward as a control reagent. All three *IGHV3-30/33* mAbs (MA1, MA6, and MA8) were NANP specific and did not bind the JR peptide according to conventional ELISA and a novel flow cytometry assay (Fig. S3 and data not shown).

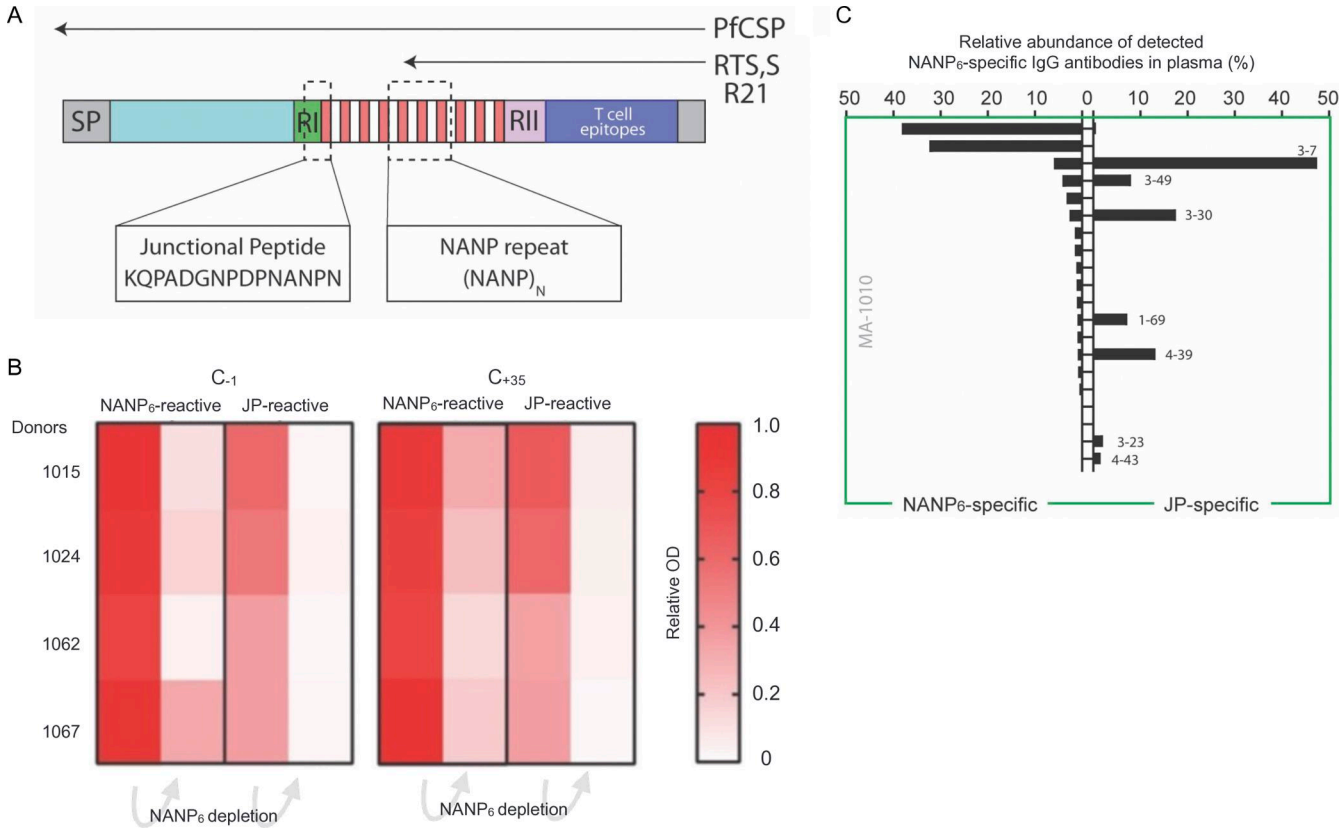

Figure 3. **R21/Matrix-M elicits polyclonal IgG plasma antibodies cross-reactive with the N-terminal JR of CSP despite its absence in the vaccine construct.** $NANP_6$ affinity chromatography depletes the plasma of JR-specific antibodies. **(A)** The schematic (A) illustrates the truncated CSP used in R21 (and RTS,S) vaccine constructs and the corresponding lack of the N-terminal JR. **(B)** Heat maps illustrate the signal loss (OD) in four VAC065 volunteers when measured by indirect ELISA using $NANP_6$ peptide or JR peptide (JR: KQPADGNPDPNANPNVDPN) after affinity chromatography and the depletion of $NANP_6$-reactive IgG from day 84 plasma at pre-challenge (C_{-1}) and post-challenge (C_{+35}) time points. **(C)** The bar graph illustrates Ig-Seq analysis of pre-challenge IgG in one volunteer (MA-1010).

MAbs MA1, MA6, and MA8 bound strongly to WT 3D7 sporozoites in an immunofluorescence assay (IFA) and to transgenic (PfCSP@PbCSP) sporozoites (Fig. 4 A). The functional capacity of MA1, MA6, and MA8 was then assessed using an in vitro model of liver-stage development using cultured human hepatocytes to measure inhibition of sporozoite invasion (ISI) activity with PfCSP@PbCSP. All mAbs tested, including 580 and 663, were able to block hepatocyte invasion, with MA1 and MA8 demonstrating a reduction in infection of 35% and 52%, respectively, while 580, 663, and MA6 all demonstrated more than

Table 2. **Summary of anti-$NANP_6$ mAbs used in this study**

mAb	CDR-H3	V_H gene	CDR-K3/L3	$V_{K/A}$ gene	IgG (%)	V_H SHM (%)	EC_{50} (nM)	Sterile protection (%)	ISI (%)	IFA (WT Pf)	IFA (Tg Pb)
MA1	ARPPPTIVGDTNNWYFGL	IGHV3-33	QSYDSSLSG	IGLV1-40	13	1.6	91	33.3	35	114	60
MA5	ARSTVEYAPGRSVWTLED	IGHV1-69	MQALQSPT	IGKV2-28	0.4	12.6	-	0	-	-	-
MA6	ARDGGHSTSWSNAFDI	IGHV3-33	QQYNSYWT	IGKV1-5	0.6	1.7	1.2	92	94	119	45
MA8	AKNAPCSGSMSCYTFDY	IGHV3-30	QQYIRYPPT	IGKV1-16	19.6	8.2	3.1	-	52	129	54
580	AKPGGDSSPAGRTWFDP	IGHV3-23	QQYYSSPIT	IGKV4-1	-	12.2	100	50	87	155	108
663	TTLLIYESDVGVDF	IGHV3-23	VQTVQVPYT	IGKV2-40	-	16.7	8.3	100	98	98	98

MA1, MA5, MA6, and MA8 were isolated from four different VAC065 volunteers. Control mAbs 580 and 663 were previously reported by Triller et al. (2017). IgG (%): the percent relative abundance of the clone's lineage in the total IgG anti-$NANP_6$ repertoire.

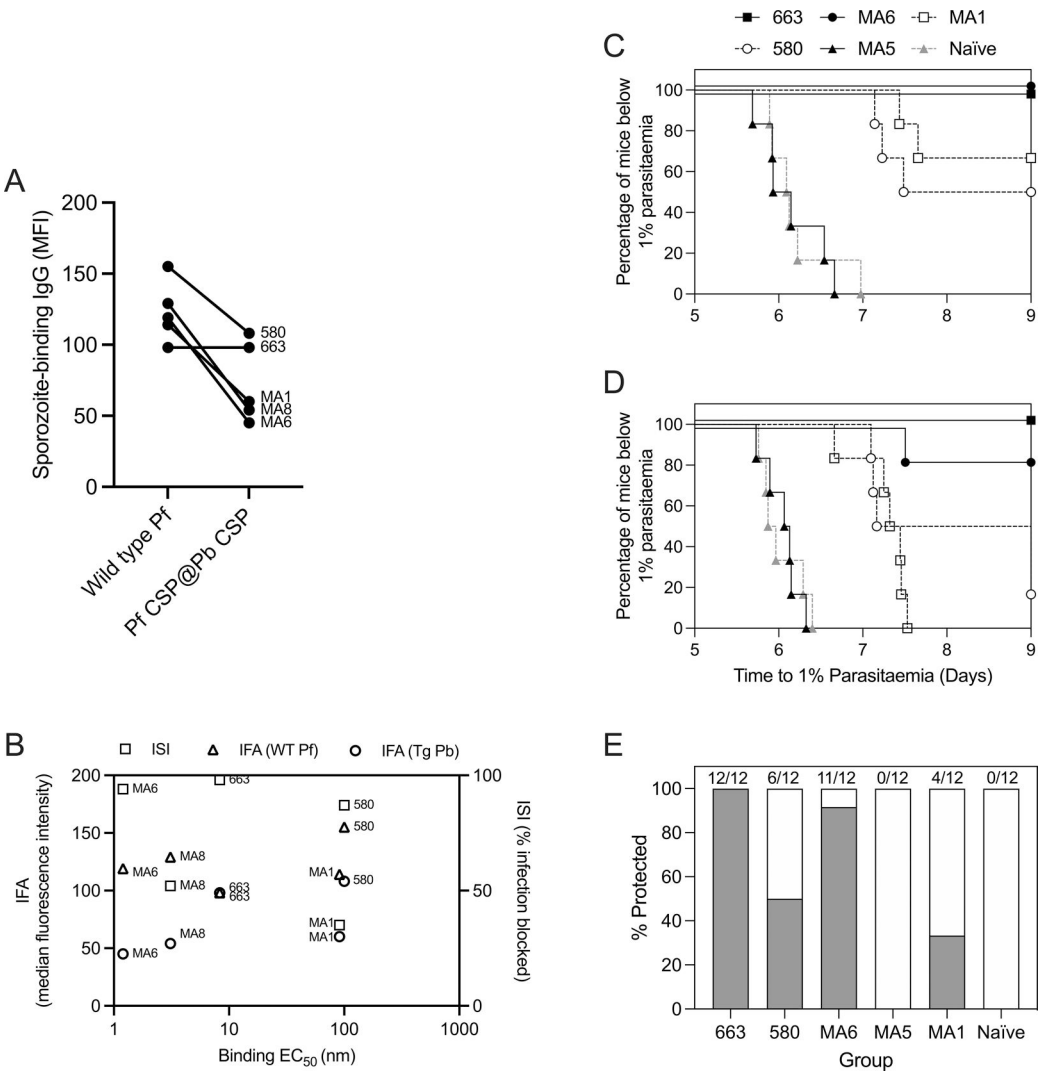

Figure 4. **Monoclonal IgG plasma antibodies elicited by R21/Matrix-M vaccine provide sterile protection in mice. (A)** Binding of mAbs to either WT 3D7 Pf (WT Pf) or transgenic Pb expressing PfCSP (Tg Pb) measured by indirect IFA. **(B)** Relationship between either IFA or ISI and NANP-binding EC_{50}. **(C and D)** C57BL/6J mice (n = 6 per group) were injected i.p. with 400 µg of mAb on day −1. The following day, mice were challenged with 5,000 Pb-PfCSP Pb sporozoites administered by s.c. injection at the base of the tail. From 5 days after sporozoite injection, mice were monitored by thin blood film for the development of blood-stage malaria. Parasitemia was calculated daily, and linear regression was used to determine the time mice reached a threshold of 1% parasitemia. Sterile protection was defined as any animal that remained parasite-free until day 9 after sporozoite administration. C and D are replicate experiments. **(E)** Summary of sterile protection for each mAb (grey bars represent the percent survival for each group over the two experiments).

85% ISI activity (Fig. 4 B). To assess the ability of plasma antibodies induced by R21/Matrix-M to confer protection in vivo, we replicated the Triller et al. (2017) experimental scheme and included mAbs 580 and 663 as references. The model employs a transgenic strain of Pb, where the endogenous PbCSP is replaced with full-length PfCSP (PfCSP@PbCSP), enabling the assessment of PfCSP mAbs within the context of natural infection in a normal mouse, as rodents are permissive for Pb infection (Espinosa et al., 2017). Female C57BL/6 mice received 400 µg of antibody i.p. and were challenged the following day with 5,000 Pb-PfCSP sporozoites.

Beginning 5 days after sporozoite injection, mice were monitored for protection against liver-stage malaria, indicated by reduction in time to develop blood-stage parasitemia or complete absence of blood-stage parasites. In two independent experiments, MA1 and 580 sterilely protected 33% and 50% of mice, respectively, compared with naïve control mice, while MA5, as expected, did not demonstrate protective immunity in this model (Fig. 4, C–E). mAb 580 demonstrated reduced efficacy (50% protection) in our model compared with 72% in the original experiment by Triller and colleagues. MA6 and 663 protected 92% and 100% of challenged mice, respectively, demonstrating potent inhibition of malaria infection. Of note, ISI appeared more closely related to in vivo protection than IFA or binding to NANP (Fig. 4, B and E).

R21/Matrix-M vaccine can elicit IgG plasma antibodies structurally homologous to those induced in B cells after sporozoite exposure

The *IGHV3-33* germline-encoded tryptophan at position 52 in CDR-H2, which can also arise in some *IGHV3-30* alleles associated

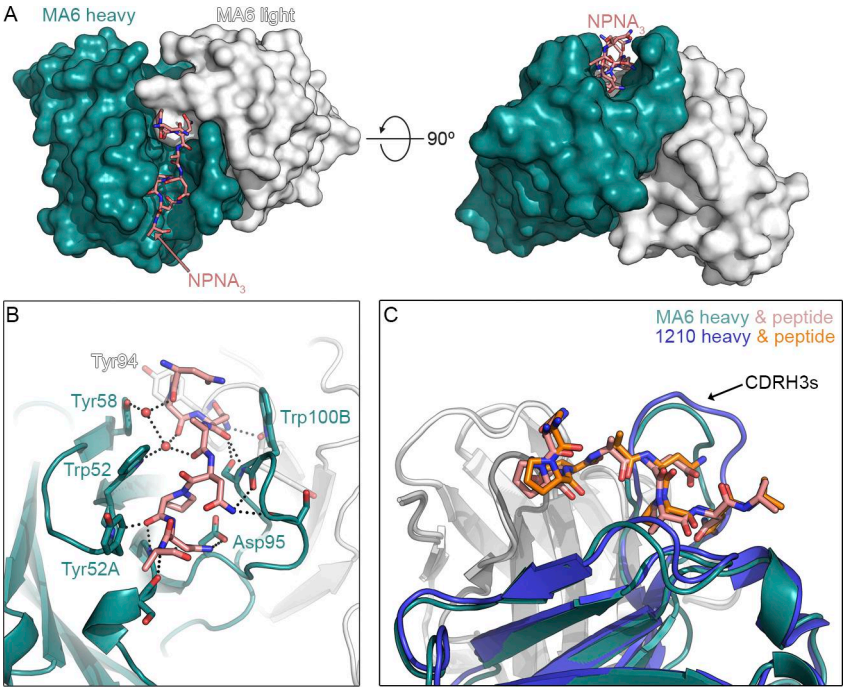

Figure 5. **Elucidation of *IGHV3-33* antibody binding modes to the NANP polypeptide.** Crystal co-structure of MA6 bound to $NPNA_3$ peptide. **(A)** Overview of peptide in groove. The peptide lies within a groove formed primarily by the heavy chain, with CDR-H3 residues forming one side of the groove and CDR-H1 and -H2 residues forming the other side. **(B)** Specific contacts. Compared to related structures, the MA6 Trp52 sidechain is flipped such that the pyrrole ring of the indole, rather than the benzene ring, packs against Pro6 of the peptide. **(C)** Superposition with 1210 F_{ab}. MA6 and 1210 bind the peptide in an almost identical conformation (RMSD of 0.23 Å for the first 8 Cα atoms).

with anti-NANP responses, plays a crucial role in antigen binding, as previously observed in several PfCSP repeat–reactive antibodies identified following immunization with sporozoites or vaccination with RTS,S/AS01 (Pholcharee et al., 2020). To further explore the molecular nature of near-germline *IGHV3-33* antibodies generated by R21/Matrix-M vaccination, we selected mAb MA6 for biophysical and structural studies (Fig. 5). Isothermal titration calorimetry experiments performed with the antigen-binding fragment (F_{ab}) of MA6 and a representative peptide of the PfCSP repeat region (Ac-NPNANPNANPNA-NH_2) resulted in a calculated binding affinity of ∼400 nM. Structural studies have clarified that anti-repeat–binding motifs are in fact DPNA, NPNV, and NPNA, which result from the combination of major and minor repeats (Dyson et al., 1990; Pholcharee et al., 2020). The MA6 F_{ab} in complex with the peptide crystallized in space group *P*21 and diffracted x-rays to a resolution of 1.8 Å. The molecular replacement solution contained two F_{ab}–peptide complexes in the asymmetric unit. Electron density for most of the peptide was well defined, allowing us to unambiguously place the first nine amino acids. The electron density for the remaining three C-terminal peptide residues was weaker, and the corresponding residues could not be placed with confidence and were omitted from the model.

The structure revealed that the peptide lies within a groove formed primarily by the heavy chain, with CDR-H3 residues forming one side of the groove and CDR-H1 and -H2 residues forming the other side (Fig. 5 A). In total, there are 701 $Å^2$ of buried surface area on the peptide, 406 $Å^2$ buried on the heavy chain, and 110 $Å^2$ buried on the light chain, with the latter interface composed entirely of the CDR-L3. CDR-H3 residue Trp100B forms Van der Waals interactions with the peptide, as do CDR-H2 residues Trp52, Tyr52A, and Tyr58. On the CDR-L3, only the sidechains of Tyr94 and Trp96 substantially contribute to the binding interface with the peptide.

In addition to the hydrophobic interactions, numerous hydrogen bonds are formed between the peptide and antibody. Several are water mediated, including those involving the sidechains of CDR-H2 residues Trp52 and Tyr58. The sidechains of CDR-H3 residues Asp95 and Ser100C both directly hydrogen bond to the peptide, but otherwise all remaining hydrogen bonds involve antibody main chain atoms. This allows for sequence variability in the antibody to be accommodated and likely explains the lack of CDR-H3 sequence conservation among similar antibodies.

Several structures of $NANP_6$-reactive antibodies in complex with peptides have been determined, including antibodies 311 and 1210 (Imkeller et al., 2018; Murugan et al., 2018; Oyen et al., 2017). Of these, antibody 1210, which was obtained from a volunteer immunized with the Sanaria PfSPZ vaccine, is most like MA6, with 89% sequence identity between the heavy chains and 96% sequence identity between the light chains. Despite this overall high sequence similarity, the MA6 CDR-H3 is substantially different from the 1210 CDR-H3, with only 5 of 14 residues in common. Yet these antibodies bind the peptide in an almost identical conformation, resulting in a root mean square deviation (RMSD) of 0.23 Å for the first eight C_α atoms. X-ray crystallography of CSP-binding antibodies has previously revealed a key structural requirement for Trp52 in the CDR-H2 of the *IGHV3-33* gene element; this feature is conserved in human mAbs 1210, MGG4, and 311, whether elicited by live sporozoites or RTS,S immunizations, as has been reviewed (Oyen et al., 2017; Pholcharee et al., 2021; Scally and Julien, 2018). Compared to other structures, the MA6 Trp52 sidechain is flipped such that the pyrrole ring of the indole, rather than the benzene ring, packs against Pro6 of the peptide. While mAb1210 and MA6 have nearly identical CDR-K3 sequences, they differ at a key residue previously identified (Imkeller et al., 2018) as critical for inter-F_{ab} interactions: mAb1210 contains Ser93, which enables

hydrogen bonding with CDR-H3, whereas MA6 retains a germline Asn at this position. Nonetheless, MA6 may still form an inter-F_{ab} hydrogen bond via its Ser99 residue in CDR-H3. Collectively, the structure of MA6 in complex with a $NPNA_3$ peptide and its comparison to the peptide-bound 1210 structure provide a molecular basis for the dominance of near-germline *IGHV3-33* $NANP_6$-reactive antibodies and their ability to accommodate diversity in their CDR-H3s.

Discussion

The robust efficacy rates observed with R21/Matrix-M at 12 mo in areas with year-round malaria transmission (Datoo et al., 2024), along with promising preliminary data at 42 mo in seasonal transmission sites, indicate that R21 is a highly efficacious vaccine with significant potential to reduce the burden of malaria. Our molecular-level analysis of the R21-generated IgG plasma antibody repertoire—showing global similarity to previously reported RTS,S B cell repertoires and validating the robust potency of these antibodies—support this conclusion.

A significant finding in this study is the dominance of NANP repeat–specific antibodies with minimal SHM in the plasma IgG repertoire induced by the R21/Matrix-M malaria vaccine. Like RTS,S-induced B cell repertoires (Oyen et al., 2017; Williams et al., 2024), the IgG plasma repertoires elicited by R21/Matrix-M also are predominantly built upon germline or near-germline *IGHV3* family genes (*IGHV3-30/3-33*). Through the cloning, functional, and structural analysis of prevalent IgG anti-NANP antibodies, we demonstrated how the R21-generated plasma antibody, MA6, inhibits sporozoite cell invasion in cell culture, curtails parasitemia, protects in a transgenic mouse model, and mediates NANP recognition through a canonical CDR-H2 Trp52 structural motif encoded by *IGHV3-33*. Since the MA6 VH region differs from the germline *IGHV3-33* gene segment by only two amino acids in its framework 2 region—neither of which interacts with $NPNA_3$ in the F_{ab}–peptide crystal structure—we speculate that MA6 originated from the naïve B cell pool and may have seeded the IgG-secreting plasma cell repertoire via a noncanonical maturation pathway. Our data suggest that repeat-specific antibodies targeting the NANP region may not undergo the extensive SHM typically seen in more mature antibody responses, instead favoring an innate-like, early stage antibody pool that is rapidly mobilized following vaccination. This speculation aligns with both recent and past observations based on RTS,S and whole-sporozoite immunizations (Murugan et al., 2018; Murugan et al., 2020; Williams et al., 2024). Furthermore, the MA6 VL region is encoded by unmutated *IGKV1-5* and contains an 8-aa long CDR-K3, akin to the public NANP-reactive "VH3-33/Vk1-5/KCDR3:8" antibody class repeatedly observed in CSP B cell repertoires (Murugan et al., 2018; Tan et al., 2018; Williams et al., 2024). Our data thus establish a connection between CSP/NANP immune responses in the naïve B cell compartment and their evolution into secreted, prevalent IgG circulating in the blood.

Notably, our study also demonstrated that CHMI challenge does not significantly boost the plasma IgG response. Despite the challenge, the quantity and composition of the NANP-reactive antibody repertoire remained stable. This finding, although counterintuitive, highlights the robust and static nature of the antibody response generated by the R21/Matrix-M vaccine. Since the elicitation of neutralizing IgG antibodies correlates with protection by vaccination for most licensed vaccines (Plotkin, 2010), and IgG anti-CSP titers meet the criteria for an immunological correlate of protection for the R21/Matrix-M vaccine (Schmit et al., 2024), we propose that the molecular profile of circulating antibodies elicited by R21/Matrix-M, as identified by Ig-Seq proteomic analysis, must reflect this fundamental biology. In this context, the temporal stability and static composition of R21-generated antibodies up to 5 wk after a sporozoite challenge infection underscore the vaccine's ability to elicit an effective sporozoite-neutralizing response. Nevertheless, titer alone could not be correlated with protection, as no significant differences were observed before challenge or after challenge in absolute (µg/ml) or relative (%) changes in titer when comparing protected and non-protected individuals. This aligns with findings from the larger phase 1–2a CHMI trial (Venkatraman et al., 2025a; Venkatraman et al., 2025b), which reported no significant difference in peak NANP-specific IgG concentrations by challenge outcome.

Among the IgG antibodies involved in the vaccine response, we found that R21/Matrix-M generates antibodies targeting the CSP JR, in addition to the CSP NANP repeat region encoded by the vaccine immunogen, representing a subset of the broader anti-$NANP_6$ repertoire. Although further studies are needed, these cross-reactive antibodies may belong to the same class as the prophylactic mAbs CIS43 and L9, which have demonstrated high efficacy in advanced clinical field trials (Kayentao et al., 2022; Kayentao et al., 2024). On the other hand, we speculate that a new class of IgG antibodies may have been missed in our analysis of R21/Matrix-M. A recent report has identified a cryptic CSP epitope—pGlu-CSP at the region I proteolytic cleavage site—on the Pf sporozoite surface as a target of protective antibodies. Notably, these potent anti-sporozoite mAbs do not bind the PfCSP central repeat region found in RTS,S/AS01 and R21/Matrix M—suggesting they are unlikely to interfere with these vaccines and might be elicited only by native sporozoites, whether as an inactivated or attenuated vaccine, or by natural infection.

For the IGHV3-30/33 NANP-specific mAbs that were tested for in vivo protection, we selected two "germline" mAbs with similar minimal SHM (MA1 and MA6, ~1.7% SHM; Table 2) to explore the relationship between binding affinity and in vivo efficacy. Notably, MA6, with nearly one order of magnitude greater binding affinity than MA1, provided the strongest protection against parasite challenge. While our data suggest that germline antibodies with higher binding affinity may offer superior in vivo protection, future studies will be needed to directly compare the affinity and in vivo efficacy of germline antibodies with mature antibodies that contain substantial somatic mutations. Such comparisons could provide further insights into the effectiveness of the R21/Matrix-M vaccine.

There are limitations to our study. Due to the separate PCR amplification of IgM versus IgG/IgA and the nonquantitative nature of our PCR method, we are unable to accurately quantify

the distribution of IgM, IgG, and IgA in our BCR-Seq libraries. We plan to address this limitation in future studies by incorporating scRNA-seq. Because our universal IgG PCR primer binds to a conserved sequence common to all IgG subclasses, it cannot distinguish between the four Fc subtypes—thereby preventing us from assessing their individual contributions to the plasmablast or serological repertoire. All cloned mAbs were expressed exclusively in IgG1 format, and we do not know whether the endogenous VH region originated from an IgG1 or from one of the other IgG subclasses (IgG2, IgG3, or IgG4).

Applying Ig-Seq antibody proteomics to analyze circulating IgG produced by the R21/Matrix-M malaria vaccine at the molecular level demonstrates the power of this technique for evaluating preerythrocytic vaccines. Furthermore, Ig-Seq offers a promising approach for unraveling lingering serological enigmas in malarial disease, such as the sporadic production of autoantibodies during acute infection (Crompton et al., 2014; Donati et al., 2004). It may also shed light on the molecular composition of circulating immune complexes implicated in cerebral malaria and severe malarial anemias (Pleass, 2009) or could offer insights into the unexpected polyclonal synergism recently described for neutralizing and non-neutralizing antibodies elicited by the strain-transcendent RH5/Matrix-M vaccine (Barrett et al., 2024; Silk et al., 2024). These insights expand our understanding of these key interactions and inform the development of future next-generation malaria vaccines.

Materials and methods

Plasma and PBMC samples

Plasma and PBMC samples were collected from 10 healthy malaria-naïve United Kingdom adult volunteers. For four volunteers, blood was drawn 7 days (day 63) following their third and final (day 56) vaccination with R21/Matrix-M (VAC053; clinicaltrials.gov identifier NCT02572388; [Venkatraman et al., 2024]). For six volunteers, blood was drawn 28 days (day 84) following their third and final (day 56) vaccination. (VAC065; clinicaltrials.gov identifier NCT02905019; [Venkatraman et al., 2025a; Venkatraman et al., 2025b]). The six VAC065 volunteers also had blood drawn 35 days (day 112) following a day 85 challenge infection by mosquito-bite transfer of Pf 3D7 sporozoites. Both clinical trials were conducted by the Jenner Institute at the University of Oxford and approved by the UK National Research Ethics Service, Committee South Central–Berkshire (16/SC/0261), the Medicines and Healthcare Products Regulatory Agency (21584/0360/001-0001), and the Oxford University Clinical Trials and Research Governance team.

High-throughput sequencing of BCR transcripts

Frozen PBMCs were thawed at 37°C, resuspended in Roswell Park Memorial Institute medium (RPMI)-1640 (Thermo Fisher Scientific) supplemented with 10% FBS and 20 U/ml deoxyribonuclease I (Roche), concentrated by centrifugation (300 × *g* for 15 min at 20°C), and allowed to recover in 4 ml media at 37°C for 30 min. The cells were then split: half were dedicated to BCR heavy chain transcript sequencing, and half were used to identify the native VHVL repertoire.

VH sequencing

Cells were diluted with 10 ml of cold buffer (PBS supplemented with 0.5% BSA and 2 mM EDTA) and pelleted via centrifugation (300 × *g* for 15 min at 4°C). The supernatant was decanted, and the cells were resuspended in 1 ml of TRIzol reagent (Thermo Fisher Scientific). RNA was extracted using RNeasy (Qiagen), and first-strand cDNA was synthesized from 500 ng total RNA using SuperScript IV (Invitrogen). IgG, IgA, and IgM heavy chain repertoires were amplified using a multiplex primer set (Ippolito et al., 2012) and sequenced by 2 × 300 paired-end Illumina MiSeq.

VH:VL paired sequencing

Total B cells were isolated from PBMCs using the Human Memory B Cell Isolation Kit (Miltenyi Biotec) with an LD column according to the manufacturer's instructions. B cells were then coemulsified with poly-dT magnetic beads and lysis buffer using a custom-designed flow-focusing device as described (McDaniel et al., 2016). VH and VL amplicons from single B cells were amplified, stitched together using overlap-extension RT-PCR, and sequenced by 2 × 300 Illumina MiSeq.

Isolation of $NANP_6$-reactive antibodies from plasma

1–2 ml plasma from each volunteer was purified with Protein G Plus agarose affinity chromatography (Thermo Fisher Scientific), and IgG $F(ab')_2$ fragments were generated with IdeS at a 1:50 ratio at 37°C for 2 h. $NANP_6$-reactive $F(ab')_2$ fragments were isolated by affinity chromatography using NeutrAvidin resin (Pierce) coupled to biotinylated $NANP_6$ peptide (ABclonal) and eluted in 100 mM glycine (pH 2.7).

Sample preparation and LC-MS/MS bioinformatic analysis

For each sample, the flow-through (nonreactive to $NANP_6$) and $NANP_6$-reactive elution were separately denatured in 1:1 (vol/vol) trifluoroethanol, reduced with 5 µl dithiothreitol (110 mM) at 55°C for 45 min, and alkylated with 32 mM iodoacetamide by incubating in the dark at room temperature (RT) for 30 min. Samples were diluted 10× into 50 mM Tris (pH 8.0) and digested with trypsin (1:10 trypsin/protein) for 3 h at 37°C. Formic acid (0.1%) was used to quench the reaction. The solution was then concentrated, desalted using a C18 Hypersep SpinTip (Thermo Fisher Scientific) according to the manufacturer's instructions, and submitted for LC-MS/MS.

Samples were submitted to the University of Texas (UT) Austin center for biomedical research (CBRS) Proteomics Facility for protein identification by LC-MS/MS using the Dionex Ultimate 3000 RSLCnano LC coupled to the Thermo Orbitrap Fusion. A 2-cm long × 75-µm I.D. C18 trap column was followed by a 75-µm I.D. × 25-cm long analytical column packed with C18 3-µm material (Thermo Acclaim PepMap 100). The FT-MS resolution was set to 120,000, and 3-s cycle time MS/MS were acquired in ion trap mode.

SEQUEST (Proteome Discoverer 1.4, Thermo Fisher Scientific) with previously described settings (Williams et al., 2017) was used to search the spectra against a patient-specific protein database constructed from the full-length VH and VL sequences, Ensembl human protein-coding sequences, and common

contaminants (https://maxquant.org). Peptide-spectrum matches (PSMs) were filtered with Percolator (Proteome Discoverer 1.4) at a false discovery rate of <1% and filtered for average mass deviations <1.5 parts per million. Peptides mapping to the CDR-H3 region of unique antibody lineages were grouped, and the relative abundances of the corresponding peptide matches were determined by the sum of the extracted ion chromatogram peak areas of the respective precursor ions, as previously described (Lavinder et al., 2014; Lee et al., 2016; Voss et al., 2021).

Antibody expression and purification

We chose mAbs that demonstrated high-confidence identification of CDR-H3 peptides in plasma via LC-MS/MS, evidenced by high abundance (indicated by the extracted ion chromatogram area) and extensive peptide coverage of the VH, particularly in the hypervariable CDR regions. Selected antibody sequences were purchased from Twist Bioscience as gene fragments cloned into a customized pcDNA3.4 vector (Invitrogen) containing human IgG1 Fc regions, IgK1 Fc regions, or IgL2 Fc regions. VH and VL plasmids were transfected into 30 ml cultures of Expi293F cells (Invitrogen) at a 1:2 ratio and incubated at 37°C and 8% CO_2 for 7 days. The supernatant containing secreted antibodies was collected following centrifugation (1,000 × *g* for 10 min at 4°C), neutralized, and filtered. Antibodies were isolated using Protein G Plus agarose (Thermo Fisher Scientific) affinity chromatography, washed with 20 column volumes of PBS, eluted with 100 mM glycine-HCl, pH 2.7, and neutralized with 1 M Tris-HCl, pH 8.0. The antibodies were then concentrated and buffer exchanged into PBS using 10,000 MWCO Vivaspin centrifugal spin columns (Sartorius).

Protein expression and purification for crystallization

The amino acid sequences for MA6 heavy and light chain variable domains were codon optimized and synthesized as gBlock gene fragments (Integrated DNA Technologies). Gene fragments were cloned into the mammalian expression plasmid pVRC8400 with an HRV 3C protease cleavage site inserted within the hinge region of the heavy chain sequence. Plasmids were used to co-transfect 0.5 L FreeStyle 293-F cells (Invitrogen) with 0.167 mg heavy chain and 0.083 mg light chain DNA using polyethylenimine 25K (Polysciences, Inc.). 6 days after transfection, cells were harvested and centrifuged at 5,400 × *g* before supernatant containing soluble protein was concentrated and buffer exchanged into PBS using a 30-kDa tangential flow filtration cassette (PALL). The sample was then passed over Pierce Protein A Plus agarose resin (Thermo Fisher Scientific) in a gravity flow column. Eluate was processed with HRV 3C protease and passed over a gravity flow column packed with CaptureSelect IgG-CH1 resin to purify the MA6 F_{ab}. A purification polishing step was then performed by passing the eluate over a Superdex 200 10/300 GL gel filtration column (Cytiva) in crystallization running buffer (2 mM Tris, pH 8.0 and 200 mM NaCl). F_{ab} peak fractions were concentrated to 11.88 mg/ml using an Amicon 30,000 molecular weight cutoff (MWCO) centrifugal spin column (EMD Millipore). $NPNA_3$ peptide (ABclonal) was solubilized in crystallization buffer (2 mM Tris, pH 8.0 and 200 mM NaCl) to a stock concentration of 500 µM.

Crystallization and data collection of MA6 in complex with $NPNA_3$

F_{ab} and $NPNA_3$ peptide were combined at a 1:12 M ratio and concentrated to 12.5 mg/ml. Crystals were produced using the sitting-drop vapor diffusion method by mixing 0.1 µl of MA6 F_{ab}–$NPNA_3$ complex with 0.05 µl of reservoir solution containing 27% PEG 3350 and 3% 2-methyl-2,4-pentanediol (MPD). The crystal was flash-cooled in liquid nitrogen directly from the crystallization drop. Diffraction data were collected to 1.8 Å from a single crystal at SBC beamline 19ID (Advanced Photon Source, Argonne National Laboratory).

Structure determination and refinement

Data were indexed and integrated in iMOSFLM (Battye et al., 2011) before being merged and scaled using Aimless (Evans and Murshudov, 2013). Molecular replacement was performed in Phaser (McCoy et al., 2007), and the model was subjected to multiple rounds of building and refinement in Coot (Emsley and Cowtan, 2004) and PHENIX (Adams et al., 2002), respectively. Data collection and refinement statistics can be found in Table 3. SBGrid (Morin et al., 2013) compiles all the crystallography processing and refinement programs used in this study.

IFA

Chambered microscope slides coated with either WT 3D7 Pf or transgenic Pb expressing PfCSP sporozoites were stored at −80°C until use. Slides were brought to RT and then fixed for 15 min in 4% paraformaldehyde. After washing twice in PBS for 5 min, slides were blocked for 1 h in casein. Slides were washed as before, and 10 µl of serum sample diluted 1:100 in casein was added to each well. Slides were incubated for 30 min at RT in a humidity chamber, then wells were individually washed with PBS three times for 5 min. Secondary antibody (anti–IgG-Alexa Fluor 488) was diluted 1:800 in casein, and 15 µl was added to each well. Slides were incubated for 30–45 min in a humidity chamber at RT protected from light. After a final wash, slides were rinsed in distilled water and left to dry before mounting with DAPI-containing media. Slides were set overnight at 4°C before being examined under a Leica DMI3000 B microscope. Images were captured in QCapturePro software using bright-field illumination, GFP, and DAPI filters at set exposure levels. ImageJ software was used to measure the median fluorescent intensity for five sporozoites in each well, and an average was taken.

ISI assay

ISI was assessed as previously described (Bowyer et al., 2018; Rodríguez-Galán et al., 2017). Human hepatoma cells (HC04 or Huh7) cultured in RPMI with 10% FBS were added to 96-well plates at 30,000 cells/well and left to settle overnight at 37°C, 5% CO_2. Viable GFP-labeled Pb sporozoites expressing PfCSP at the Pb CSP locus (Pb PfCSP@PbCSP) were obtained by dissecting infected *A. stephensi* mosquitoes. Dissected salivary glands were pooled into RPMI 1640. Culture medium was aspirated from the

Table 3. **MA6 F_{ab} + $NPNA_3$ data collection and refinement statistics**

PDB ID	9CR9
Data collection	
Wavelength (Å)	0.9795
Resolution range	47.72–1.8 (1.864–1.8)
Space group	$P\ 1\ 2_1\ 1$
Unit cell dimensions	
a, *b*, *c* (Å)	46.6, 61.0, 153.0
α, β, γ (°)	90, 90, 90
Total reflections	137,629 (13,558)
Unique reflections	74,608 (7,426)
Multiplicity	1.8 (1.8)
Completeness (%)	93.3 (93.1)
I/σI	5.93 (2.14)
Wilson B-factor	17.1
R_{merge}	0.077 (0.4335)
$CC_{1/2}$	0.941 (0.626)
Refinement	
Unique reflections	74,522 (7,401)
R_{work}	0.1853 (0.2749)
R_{free}	0.2153 (0.3039)
Number of non-hydrogen atoms	7,814
Macromolecules	6,652
Ligands	0
Solvent	1,162
Protein residues	872
RMSD bond lengths (Å)	0.008
RMSD bond angles (°)	0.96
Ramachandran favored (%)	98.36
Ramachandran allowed (%)	1.64
Ramachandran outliers (%)	0.00
Rotamer outliers (%)	0.00
Clashscore	4.05
Average B-factor (Å^2)	23.9
Macromolecules	22.1
Solvent	34.1

Statistics for the highest resolution shell are shown in parentheses. PDB, Protein Data Bank.

hepatoma cells, then 100 µl of serum diluted 1:5 in RPMI with 10% FBS, and 100 µl of sporozoite solution (10,000 sporozoites) were added to each well, giving a 10% final serum concentration. Samples were tested in duplicate: "hepatoma only" wells and positive control wells containing hepatoma cells and sporozoites, but no serum, were included. Baseline (pre-vaccination) and post-vaccination samples were run for each volunteer tested. After incubation for 20–26 h at 37°C, media was aspirated and plates were washed with 90 µl/well DPBS. Cells were trypsinized, resuspended in 65 µl DPBS with 1% BSA, and acquired immediately using a BD LSR II and FACSDiva v6.2. DAPI stain was added to each sample just before acquisition. Data were analyzed in FlowJo software v10.6 (TreeStar, Inc.).

Protection study in mice

Mice were used in accordance with the UK Animals (Scientific Procedures) Act under project license number P9804B4F1 granted by the UK Home Office following ethical review by the University of Oxford Animal Welfare and Ethical Review Board. Animals were group housed in individually ventilated cages under specific pathogen–free conditions, with constant temperature and humidity and lighting on a 13:11 (7 am to 8 pm) light–dark cycle. Each mouse received 400 µg of mAb i.p. injection the day before challenge with 5,000 Pb-PfCSP sporozoites.

Pb sporozoites expressing PfCSP under the control of the PbCSP promoter (Pb-PfCSP) (Rodríguez-Galán et al., 2017) were isolated from salivary glands of female *A. stephensi* mosquitoes around 21 days after feeding on a Pb-PfCSP blood stage infected donor mouse. Salivary glands were homogenized, sporozoites counted under phase contrast microscopy, and 5,000 Pb-PfCSP sporozoites injected s.c. into recipient mice. Mice were monitored daily from day 5 onward by taking a thin blood film and staining with 5% Giemsa (Sigma-Aldrich) to screen for the presence of schizonts within the red blood cells. Parasitemia was calculated as the percentage of infected red blood cells per microscope field (100× objective), with at least five fields counted per mouse per day. Using linear regression, the time to 1% parasitemia was calculated based on the y-intercept and slope of the line.

Statistical analysis

Nonparametric Mann–Whitney U test was used to compare two groups. Two-tailed Kruskal–Wallis test followed by Dunn's multiple comparisons test was used to compare groups of three or more. Kaplan–Meier survival analysis was tested by the log-rank test. Sample sizes for each experiment were based on a power calculation and/or previous experience of the mouse models. Data analysis and visualization were performed using GraphPad Prism, Microsoft Excel, Microsoft PowerPoint, Adobe Illustrator, Immunarch, and R Studio. P values <0.05 were considered statistically significant.

Online supplemental material

Fig. S1 shows the profile of $NANP_6$-reactive IgG repertoires across all 10 volunteers after vaccination, indicating number of IgG lineages per volunteer, frequency of CDR-H3 lengths for all lineages, dissimilarity of VH repertoires according to tSNE analysis, and frequency of IGHV gene use by volunteer. Fig. S2 shows the composition and correlation between NANP6 pre-challenge and post-challenge IgG repertoires among VAC065 volunteers. Fig. S3 shows the epitope specificity of MA6 mAb by flow cytometry. Table S1 shows the R21 Ig-Seq repertoire summaries for each subject.

Data availability

Sequence data are openly available in a public repository. Raw Illumina sequencing reads for natively paired VH:VL and

VH-only BCR sequences (BCR-Seq) have been deposited at NCBI Sequence Read Archive under BioProject ID PRJNA1216750 and are publicly available as of the date of publication. Raw LC-MS/MS data for plasma IgG proteomics (Ig-Seq) have been deposited to the MassIVE proteomics repository (dataset MSV000096964) and are publicly available as of the date of publication. The mAbs have been deposited to GenBank with accession numbers PV667658–PV667665. Coordinates for the MA6 Fab in complex with NANP3 peptide have been deposited to the Protein Data Bank under accession no. 9CR9. All other data are presented in the figures and supplementary materials.

Acknowledgments

NGS was performed by the Genomic Sequencing and Analysis Facility at UT Austin, Center for Biomedical Research Support, RRID#: SCR_021713. Mass spectrometry was performed by the Biological Mass Spectrometry Facility at UT Austin. The authors acknowledge the Texas Advanced Computing Center at UT Austin for providing high-performance computing resources that have contributed to the research results reported within this paper.

This work was funded by PATH's Center for Vaccine Innovation and Access, through a grant awarded to PATH by the Bill & Melinda Gates Foundation (INV-007217), under a collaborative agreement with The Jenner Institute at the University of Oxford (K.J. Ewer) and UT Austin (G.C. Ippolito). This work was partly funded by Welch Foundation grant number F-0003-19620604 (J.S. McLellan). Open Access funding provided by the University of Oxford.

Author contributions: J.R. McDaniel: conceptualization, data curation, formal analysis, investigation, methodology, software, validation, visualization, and writing—original draft, review, and editing. W.N. Voss: formal analysis, investigation, visualization, and writing—original draft, review, and editing. G. Bowyer: conceptualization, data curation, formal analysis, investigation, visualization, and writing—review and editing. S.A. Rush: formal analysis, investigation, visualization, and writing—original draft. A.J. Spencer: formal analysis, investigation, methodology, resources, and writing—review and editing. D.G. Bellamy: investigation. M. Ulaszewska: resources. J. Goike: investigation. S. Gregory: project administration. C.R. King: conceptualization, funding acquisition, investigation, and writing—review and editing. J. McLellan: investigation, resources, supervision, validation, visualization, and writing—review and editing. A.V.S. Hill: funding acquisition, project administration, resources, supervision, and writing—review and editing. G. Georgiou: conceptualization, funding acquisition, and supervision. K.J. Ewer: formal analysis, funding acquisition, resources, supervision, visualization, and writing—original draft, review, and editing. G.C. Ippolito: conceptualization, formal analysis, funding acquisition, investigation, methodology, project administration, supervision, validation, visualization, and writing—original draft, review, and editing.

Disclosures: G. Bowyer reported other from AstraZeneca outside the submitted work, and is an employee of AstraZeneca. A.V.S. Hill reported other from University of Oxford during the conduct of the study; grants from Serum Institute of India outside the submitted work; and had a patent to US Patent no. US 9821046 and related patents in other territories with royalties paid (Serum Institute of India). G. Georgiou reported patent no. 9,708,654 with royalties paid (Griffols) and patent no. 10,175,249 with royalties paid (Cell Signaling Technologies). K.J. Ewer reported a patent to R21 vaccine IP issued to University of Oxford with royalties paid (Serum Institute India PL), was an employee of the University of Oxford at the time of the work, and is now an employee of GSK. K.J. Ewer owns restricted shares in GSK. No other disclosures were reported.

Submitted: 14 October 2024
Revised: 10 February 2025
Accepted: 23 June 2025

References

Adams, P.D., R.W. Grosse-Kunstleve, L.W. Hung, T.R. Ioerger, A.J. McCoy, N.W. Moriarty, R.J. Read, J.C. Sacchettini, N.K. Sauter, and T.C. Terwilliger. 2002. PHENIX: Building new software for automated crystallographic structure determination. *Acta Crystallogr. D Biol. Crystallogr.* 58:1948–1954. https://doi.org/10.1107/s0907444902016657

Barrett, J.R., D. Pipini, N.D. Wright, A.J.R. Cooper, G. Gorini, D. Quinkert, A.M. Lias, H. Davies, C.A. Rigby, M. Aleshnick, et al. 2024. Analysis of the diverse antigenic landscape of the malaria protein RH5 identifies a potent vaccine-induced human public antibody clonotype. *Cell*. 187: 4964–4980.e21. https://doi.org/10.1016/j.cell.2024.06.015

Battye, T.G.G., L. Kontogiannis, O. Johnson, H.R. Powell, and A.G.W. Leslie. 2011. iMOSFLM: a new graphical interface for diffraction-image processing with MOSFLM. *Acta Crystallogr. D Biol. Crystallogr.* 67:271–281. https://doi.org/10.1107/S0907444910048675

Bondt, A., M. Hoek, S. Tamara, B. de Graaf, W. Peng, D. Schulte, D.M.H. van Rijswijck, M.A. den Boer, J.F. Greisch, M.R.J. Varkila, et al. 2021. Human plasma IgG1 repertoires are simple, unique, and dynamic. *Cell Syst.* 12: 1131–1143.e5. https://doi.org/10.1016/j.cels.2021.08.008

Bowyer, G., A. Grobbelaar, T. Rampling, N. Venkatraman, D. Morelle, R.W. Ballou, A.V.S. Hill, and K.J. Ewer. 2018. CXCR3+ T follicular helper cells induced by Co-administration of RTS,S/AS01B and viral-vectored vaccines are associated with reduced immunogenicity and efficacy against malaria. *Front. Immunol.* 9:1660. https://doi.org/10.3389/fimmu.2018.01660

Collins, K.A., R. Snaith, M.G. Cottingham, S.C. Gilbert, and A.V.S. Hill. 2017. Enhancing protective immunity to malaria with a highly immunogenic virus-like particle vaccine. *Sci. Rep.* 7:46621. https://doi.org/10.1038/srep46621

Crompton, P.D., J. Moebius, S. Portugal, M. Waisberg, G. Hart, L.S. Garver, L.H. Miller, C. Barillas-Mury, and S.K. Pierce. 2014. Malaria immunity in man and mosquito: Insights into unsolved mysteries of a deadly infectious disease. *Annu. Rev. Immunol.* 32:157–187. https://doi.org/10.1146/annurev-immunol-032713-120220

Dame, J.B., J.L. Williams, T.F. McCutchan, J.L. Weber, R.A. Wirtz, W.T. Hockmeyer, W.L. Maloy, J.D. Haynes, I. Schneider, and D. Roberts. 1984. Structure of the gene encoding the immunodominant surface antigen on the sporozoite of the human malaria parasite Plasmodium falciparum. *Science*. 225:593–599. https://doi.org/10.1126/science.6204383

Datoo, M.S., A. Dicko, H. Tinto, J.B. Ouédraogo, M. Hamaluba, A. Olotu, E. Beaumont, F. Ramos Lopez, H.M. Natama, S. Weston, et al. 2024. Safety and efficacy of malaria vaccine candidate R21/Matrix-M in African children: A multicentre, double-blind, randomised, phase 3 trial. *Lancet*. 403:533–544. https://doi.org/10.1016/S0140-6736(23)02511-4

de Graaf, S.C., M. Hoek, S. Tamara, and A.J.R. Heck. 2022. A perspective toward mass spectrometry-based de novo sequencing of endogenous antibodies. *MAbs*. 14:2079449. https://doi.org/10.1080/19420862.2022.2079449

Donati, D., L.P. Zhang, A. Chêne, Q. Chen, K. Flick, M. Nyström, M. Wahlgren, and M.T. Bejarano. 2004. Identification of a polyclonal B-cell activator in Plasmodium falciparum. *Infect. Immun.* 72:5412–5418. https://doi.org/10.1128/IAI.72.9.5412-5418.2004

Dyson, H.J., A.C. Satterthwait, R.A. Lerner, and P.E. Wright. 1990. Conformational preferences of synthetic peptides derived from the immunodominant site of the circumsporozoite protein of Plasmodium falciparum by 1H NMR. *Biochemistry*. 29:7828–7837. https://doi.org/10.1021/bi00486a008

Emsley, P., and K. Cowtan. 2004. Coot: Model-building tools for molecular graphics. *Acta Crystallogr. D Biol. Crystallogr.* 60:2126–2132. https://doi.org/10.1107/S0907444904019158

Espinosa, D.A., D. Christensen, C. Muñoz, S. Singh, E. Locke, P. Andersen, and F. Zavala. 2017. Robust antibody and CD8$^+$ T-cell responses induced by P. falciparum CSP adsorbed to cationic liposomal adjuvant CAF09 confer sterilizing immunity against experimental rodent malaria infection. *NPJ Vaccines* 2:10. https://doi.org/10.1038/s41541-017-0011-y

Evans, P.R., and G.N. Murshudov. 2013. How good are my data and what is the resolution? *Acta Crystallogr. D Biol. Crystallogr.* 69:1204–1214. https://doi.org/10.1107/S0907444913000061

Foquet, L., C.C. Hermsen, G.J. van Gemert, E. Van Braeckel, K.E. Weening, R. Sauerwein, P. Meuleman, and G. Leroux-Roels. 2014. Vaccine-induced monoclonal antibodies targeting circumsporozoite protein prevent Plasmodium falciparum infection. *J. Clin. Invest.* 124:140–144. https://doi.org/10.1172/JCI70349

Hill, A.V.S. 2006. Pre-erythrocytic malaria vaccines: Towards greater efficacy. *Nat. Rev. Immunol.* 6:21–32. https://doi.org/10.1038/nri1746

Hollingdale, M.R., E.H. Nardin, S. Tharavanij, A.L. Schwartz, and R.S. Nussenzweig. 1984. Inhibition of entry of Plasmodium falciparum and P. vivax sporozoites into cultured cells; an in vitro assay of protective antibodies. *J. Immunol.* 132:909–913.

Imkeller, K., S.W. Scally, A. Bosch, G.P. Martí, G. Costa, G. Triller, R. Murugan, V. Renna, H. Jumaa, P.G. Kremsner, et al. 2018. Antihomotypic affinity maturation improves human B cell responses against a repetitive epitope. *Science*. 360:1358–1362. https://doi.org/10.1126/science.aar5304

Ippolito, G.C., R.L. Schelonka, M. Zemlin, I.I. Ivanov, R. Kobayashi, C. Zemlin, G.L. Gartland, L. Nitschke, J. Pelkonen, K. Fujihashi, et al. 2006. Forced usage of positively charged amino acids in immunoglobulin CDR-H3 impairs B cell development and antibody production. *J. Exp. Med.* 203:1567–1578. https://doi.org/10.1084/jem.20052217

Ippolito, G.C., K.H. Hoi, S.T. Reddy, S.M. Carroll, X. Ge, T. Rogosch, M. Zemlin, L.D. Shultz, A.D. Ellington, C.L. Vandenberg, et al. 2012. Antibody repertoires in humanized NOD-scid-IL2Rγ(null) mice and human B cells reveals human-like diversification and tolerance checkpoints in the mouse. *PLoS One*. 7:e35497. https://doi.org/10.1371/journal.pone.0035497

Julien, J.P., and H. Wardemann. 2019. Antibodies against Plasmodium falciparum malaria at the molecular level. *Nat. Rev. Immunol.* 19:761–775. https://doi.org/10.1038/s41577-019-0209-5

Kappe, S.H.I., C.A. Buscaglia, and V. Nussenzweig. 2004. Plasmodium sporozoite molecular cell biology. *Annu. Rev. Cell Dev. Biol.* 20:29–59. https://doi.org/10.1146/annurev.cellbio.20.011603.150935

Kayentao, K., A. Ongoiba, A.C. Preston, S.A. Healy, S. Doumbo, D. Doumtabe, A. Traore, H. Traore, A. Djiguiba, S. Li, et al. 2022. Safety and efficacy of a monoclonal antibody against malaria in Mali. *N. Engl. J. Med.* 387:1833–1842. https://doi.org/10.1056/NEJMoa2206966

Kayentao, K., A. Ongoiba, A.C. Preston, S.A. Healy, Z. Hu, J. Skinner, S. Doumbo, J. Wang, H. Cisse, D. Doumtabe, et al. 2024. Subcutaneous administration of a monoclonal antibody to prevent malaria. *N. Engl. J. Med.* 390:1549–1559. https://doi.org/10.1056/NEJMoa2312775

Kisalu, N.K., A.H. Idris, C. Weidle, Y. Flores-Garcia, B.J. Flynn, B.K. Sack, S. Murphy, A. Schön, E. Freire, J.R. Francica, et al. 2018. A human monoclonal antibody prevents malaria infection by targeting a new site of vulnerability on the parasite. *Nat. Med.* 24:408–416. https://doi.org/10.1038/nm.4512

Lavinder, J.J., A.P. Horton, G. Georgiou, and G.C. Ippolito. 2015. Next-generation sequencing and protein mass spectrometry for the comprehensive analysis of human cellular and serum antibody repertoires. *Curr. Opin. Chem. Biol.* 24:112–120. https://doi.org/10.1016/j.cbpa.2014.11.007

Lavinder, J.J., Y. Wine, C. Giesecke, G.C. Ippolito, A.P. Horton, O.I. Lungu, K.H. Hoi, B.J. DeKosky, E.M. Murrin, M.M. Wirth, et al. 2014. Identification and characterization of the constituent human serum antibodies elicited by vaccination. *Proc. Natl. Acad. Sci. USA*. 111:2259–2264. https://doi.org/10.1073/pnas.1317793111

Lee, J., D.R. Boutz, V. Chromikova, M.G. Joyce, C. Vollmers, K. Leung, A.P. Horton, B.J. DeKosky, C.H. Lee, J.J. Lavinder, et al. 2016. Molecular-level analysis of the serum antibody repertoire in young adults before and after seasonal influenza vaccination. *Nat. Med.* 22:1456–1464. https://doi.org/10.1038/nm.4224

McCoy, A.J., R.W. Grosse-Kunstleve, P.D. Adams, M.D. Winn, L.C. Storoni, and R.J. Read. 2007. Phaser crystallographic software. *J. Appl. Crystallogr.* 40:658–674. https://doi.org/10.1107/S0021889807021206

McDaniel, J.R., B.J. DeKosky, H. Tanno, A.D. Ellington, and G. Georgiou. 2016. Ultra-high-throughput sequencing of the immune receptor repertoire from millions of lymphocytes. *Nat. Protoc.* 11:429–442. https://doi.org/10.1038/nprot.2016.024

Miura, K., Y. Flores-Garcia, C.A. Long, and F. Zavala. 2024. Vaccines and monoclonal antibodies: New tools for malaria control. *Clin. Microbiol. Rev.* 37:e0007123. https://doi.org/10.1128/cmr.00071-23

Moorthy, V., M.J. Hamel, and P.G. Smith. 2024. Malaria vaccines for children: And now there are two. *Lancet*. 403:504–505. https://doi.org/10.1016/S0140-6736(23)02743-5

Morin, A., B. Eisenbraun, J. Key, P.C. Sanschagrin, M.A. Timony, M. Ottaviano, and P. Sliz. 2013. Collaboration gets the most out of software. *Elife*. 2:e01456. https://doi.org/10.7554/eLife.01456

Murugan, R., L. Buchauer, G. Triller, C. Kreschel, G. Costa, G. Pidelaserra Martí, K. Imkeller, C.E. Busse, S. Chakravarty, B.K.L. Sim, et al. 2018. Clonal selection drives protective memory B cell responses in controlled human malaria infection. *Sci. Immunol.* 3:eaap8029. https://doi.org/10.1126/sciimmunol.aap8029

Murugan, R., S.W. Scally, G. Costa, G. Mustafa, E. Thai, T. Decker, A. Bosch, K. Prieto, E.A. Levashina, J.P. Julien, and H. Wardemann. 2020. Evolution of protective human antibodies against Plasmodium falciparum circumsporozoite protein repeat motifs. *Nat. Med.* 26:1135-1145, https://doi.org/10.1038/s41591-020-0881-9

Nnaji, C.A., U.A. Amaechi, and C.S. Wiysonge. 2024. R21/Matrix-M vaccine: Optimising supply, maximising impact. *Lancet*. 403:525. https://doi.org/10.1016/S0140-6736(23)02716-2

Nussenzweig, R.S., and V. Nussenzweig. 1989. Antisporozoite vaccine for malaria: Experimental basis and current status. *Rev. Infect. Dis.* 11:S579–S585. https://doi.org/10.1093/clinids/11.supplement_3.s579

Oyen, D., J.L. Torres, P.C. Aoto, Y. Flores-Garcia, Š. Binter, T. Pholcharee, S. Carroll, S. Reponen, R. Wash, Q. Liang, et al. 2020. Structure and mechanism of monoclonal antibody binding to the junctional epitope of Plasmodium falciparum circumsporozoite protein. *PLoS Pathog.* 16:e1008373. https://doi.org/10.1371/journal.ppat.1008373

Oyen, D., J.L. Torres, U. Wille-Reece, C.F. Ockenhouse, D. Emerling, J. Glanville, W. Volkmuth, Y. Flores-Garcia, F. Zavala, A.B. Ward, et al. 2017. Structural basis for antibody recognition of the NANP repeats in *Plasmodium falciparum* circumsporozoite protein. *Proc. Natl. Acad. Sci. USA*. 114:E10438–E10445. https://doi.org/10.1073/pnas.1715812114

Pholcharee, T., D. Oyen, Y. Flores-Garcia, G. Gonzalez-Paez, Z. Han, K.L. Williams, W. Volkmuth, D. Emerling, E. Locke, C. Richter King, et al. 2021. Structural and biophysical correlation of anti-NANP antibodies with in vivo protection against P. falciparum. *Nat. Commun.* 12:1063. https://doi.org/10.1038/s41467-021-21221-4

Pholcharee, T., D. Oyen, J.L. Torres, Y. Flores-Garcia, G.M. Martin, G.E. González-Páez, D. Emerling, W. Volkmuth, E. Locke, C.R. King, et al. 2020. Diverse antibody responses to conserved structural motifs in Plasmodium falciparum circumsporozoite protein. *J. Mol. Biol.* 432:1048–1063. https://doi.org/10.1016/j.jmb.2019.12.029

Pleass, R.J. 2009. When is a malaria immune complex not an immune complex? *Parasite Immunol.* 31:61–63. https://doi.org/10.1111/j.1365-3024.2008.01076.x

Plotkin, S.A. 2010. Correlates of protection induced by vaccination. *Clin. Vaccine Immunol.* 17:1055–1065. https://doi.org/10.1128/CVI.00131-10

Rodríguez-Galán, A., A.M. Salman, G. Bowyer, K.A. Collins, R.J. Longley, F. Brod, M. Ulaszewska, K.J. Ewer, C.J. Janse, S.M. Khan, et al. 2017. An in vitro assay to measure antibody-mediated inhibition of P. berghei sporozoite invasion against P. falciparum antigens. *Sci. Rep.* 7:17011. https://doi.org/10.1038/s41598-017-17274-5

Scally, S.W., and J.P. Julien. 2018. Peek-Peak-Pique: Repeating motifs of subtle variance are targets for potent malaria antibodies. *Immunity*. 48:851–854. https://doi.org/10.1016/j.immuni.2018.04.037

Schmit, N., H.M. Topazian, H.M. Natama, D. Bellamy, O. Traoré, M.A. Somé, T. Rouamba, M.C. Tahita, M.D.A. Bonko, A. Sourabié, et al. 2024. The public health impact and cost-effectiveness of the R21/Matrix-M malaria vaccine: A mathematical modelling study. *Lancet Infect. Dis.* 24:465–475. https://doi.org/10.1016/S1473-3099(23)00816-2

Schulte, D., W. Peng, and J. Snijder. 2022. Template-based assembly of proteomic short reads for *de novo* antibody sequencing and repertoire profiling. *Anal. Chem.* 94:10391–10399. https://doi.org/10.1021/acs.analchem.2c01300

Silk, S.E., W.F. Kalinga, J. Salkeld, I.M. Mtaka, S. Ahmed, F. Milando, A. Diouf, C.K. Bundi, N. Balige, O. Hassan, et al. 2024. Blood-stage malaria vaccine

candidate RH5.1/Matrix-M in healthy Tanzanian adults and children; an open-label, non-randomised, first-in-human, single-centre, phase 1b trial. *Lancet Infect. Dis.* 24:1105–1117. https://doi.org/10.1016/S1473-3099(24)00312-8

Stoute, J.A., M. Slaoui, D.G. Heppner, P. Momin, K.E. Kester, P. Desmons, B.T. Wellde, N. Garçon, U. Krzych, and M. Marchand. 1997. A preliminary evaluation of a recombinant circumsporozoite protein vaccine against Plasmodium falciparum malaria. RTS,S Malaria Vaccine Evaluation Group. *N. Engl. J. Med.* 336:86–91. https://doi.org/10.1056/NEJM199701093360202

Tan, J., B.K. Sack, D. Oyen, I. Zenklusen, L. Piccoli, S. Barbieri, M. Foglierini, C.S. Fregni, J. Marcandalli, S. Jongo, et al. 2018. A public antibody lineage that potently inhibits malaria infection through dual binding to the circumsporozoite protein. *Nat. Med.* 24:401–407. https://doi.org/10.1038/nm.4513

Townsend, D.R., D.M. Towers, J.J. Lavinder, and G.C. Ippolito. 2024. Innovations and trends in antibody repertoire analysis. *Curr. Opin. Biotechnol.* 86:103082. https://doi.org/10.1016/j.copbio.2024.103082

Triller, G., S.W. Scally, G. Costa, M. Pissarev, C. Kreschel, A. Bosch, E. Marois, B.K. Sack, R. Murugan, A.M. Salman, et al. 2017. Natural parasite exposure induces protective human anti-malarial antibodies. *Immunity*. 47:1197–1209.e10. https://doi.org/10.1016/j.immuni.2017.11.007

Ubillos, I., A. Ayestaran, A.J. Nhabomba, D. Dosoo, M. Vidal, A. Jiménez, C. Jairoce, H. Sanz, R. Aguilar, N.A. Williams, et al. 2018. Baseline exposure, antibody subclass, and hepatitis B response differentially affect malaria protective immunity following RTS,S/AS01E vaccination in African children. *BMC Med.* 16:197. https://doi.org/10.1186/s12916-018-1186-4

Venkatesan, P. 2024. The 2023 WHO World malaria report. *Lancet Microbe*. 5:e214. https://doi.org/10.1016/S2666-5247(24)00016-8

Venkatraman, N., D. Silman, D. Bellamy, L. Stockdale, G. Bowyer, N.J. Edwards, O. Griffiths, F.R. Lopez, J. Powlson, C. Mair, et al. 2025a. R21 in Matrix-M adjuvant in UK malaria-naive adult men and non-pregnant women aged 18-45 years: An open-label, partially blinded, phase 1-2a controlled human malaria infection study. *Lancet Microbe*. 6:100867. https://doi.org/10.1016/S2666-5247(24)00083-1

Venkatraman, N., A.B. Tiono, G. Bowyer, D.G. Bellamy, L.K. Stockdale, J. Powlson, K.A. Collins, S. Coulibaly, M.S. Datoo, D. Silman, et al. 2025b. Evaluation of a novel malaria anti-sporozoite vaccine candidate, R21 in Matrix-M adjuvant, in the UK and Burkina Faso: Two phase 1, first-in-human trials. *Lancet Microbe*. 6:100868. https://doi.org/10.1016/S2666-5247(24)00084-3

Voss, W.N., Y.J. Hou, N.V. Johnson, G. Delidakis, J.E. Kim, K. Javanmardi, A.P. Horton, F. Bartzoka, C.J. Paresi, Y. Tanno, et al. 2021. Prevalent, protective, and convergent IgG recognition of SARS-CoV-2 non-RBD spike epitopes. *Science*. 372:1108–1112. https://doi.org/10.1126/science.abg5268

Wahl, I., and H. Wardemann. 2022. How to induce protective humoral immunity against Plasmodium falciparum circumsporozoite protein. *J. Exp. Med.* 219:e20201313. https://doi.org/10.1084/jem.20201313

Wang, L.T., L.S. Pereira, Y. Flores-Garcia, J. O'Connor, B.J. Flynn, A. Schön, N.K. Hurlburt, M. Dillon, A.S.P. Yang, A. Fabra-García, et al. 2020. A potent anti-malarial human monoclonal antibody targets circumsporozoite protein minor repeats and neutralizes sporozoites in the liver. *Immunity*. 53:733–744.e8. https://doi.org/10.1016/j.immuni.2020.08.014

Wang, R., Y. Charoenvit, G. Corradin, R. Porrozzi, R.L. Hunter, G. Glenn, C.R. Alving, P. Church, and S.L. Hoffman. 1995. Induction of protective polyclonal antibodies by immunization with a Plasmodium yoelii circumsporozoite protein multiple antigen peptide vaccine. *J. Immunol.* 154:2784–2793.

White, M.T., R. Verity, J.T. Griffin, K.P. Asante, S. Owusu-Agyei, B. Greenwood, C. Drakeley, S. Gesase, J. Lusingu, D. Ansong, et al. 2015. Immunogenicity of the RTS,S/AS01 malaria vaccine and implications for duration of vaccine efficacy: Secondary analysis of data from a phase 3 randomised controlled trial. *Lancet Infect. Dis.* 15:1450–1458. https://doi.org/10.1016/S1473-3099(15)00239-X

Williams, K.L., S. Guerrero, Y. Flores-Garcia, D. Kim, K.S. Williamson, C. Siska, P. Smidt, S.Z. Jepson, K. Li, S.M. Dennison, et al. 2024. A candidate antibody drug for prevention of malaria. *Nat. Med.* 30:117–129. https://doi.org/10.1038/s41591-023-02659-z

Williams, L.D., G. Ofek, S. Schätzle, J.R. McDaniel, X. Lu, N.I. Nicely, L. Wu, C.S. Lougheed, T. Bradley, M.K. Louder, et al. 2017. Potent and broad HIV-neutralizing antibodies in memory B cells and plasma. *Sci. Immunol.* 2:eaal2200. https://doi.org/10.1126/sciimmunol.aal2200

Xu, J.L., and M.M. Davis. 2000. Diversity in the CDR3 region of V(H) is sufficient for most antibody specificities. *Immunity*. 13:37–45. https://doi.org/10.1016/s1074-7613(00)00006-6

Zavala, F. 2022. RTS,S: The first malaria vaccine. *J. Clin. Invest* 132:e156588. https://doi.org/10.1172/JCI156588

Zavala, F., and S. Chai. 1990. Protective anti-sporozoite antibodies induced by a chemically defined synthetic vaccine. *Immunol. Lett.* 25:271–274. https://doi.org/10.1016/0165-2478(90)90126-b

Zavala, F., A.H. Cochrane, E.H. Nardin, R.S. Nussenzweig, and V. Nussenzweig. 1983. Circumsporozoite proteins of malaria parasites contain a single immunodominant region with two or more identical epitopes. *J. Exp. Med.* 157:1947–1957. https://doi.org/10.1084/jem.157.6.1947

JEM

Supplemental material

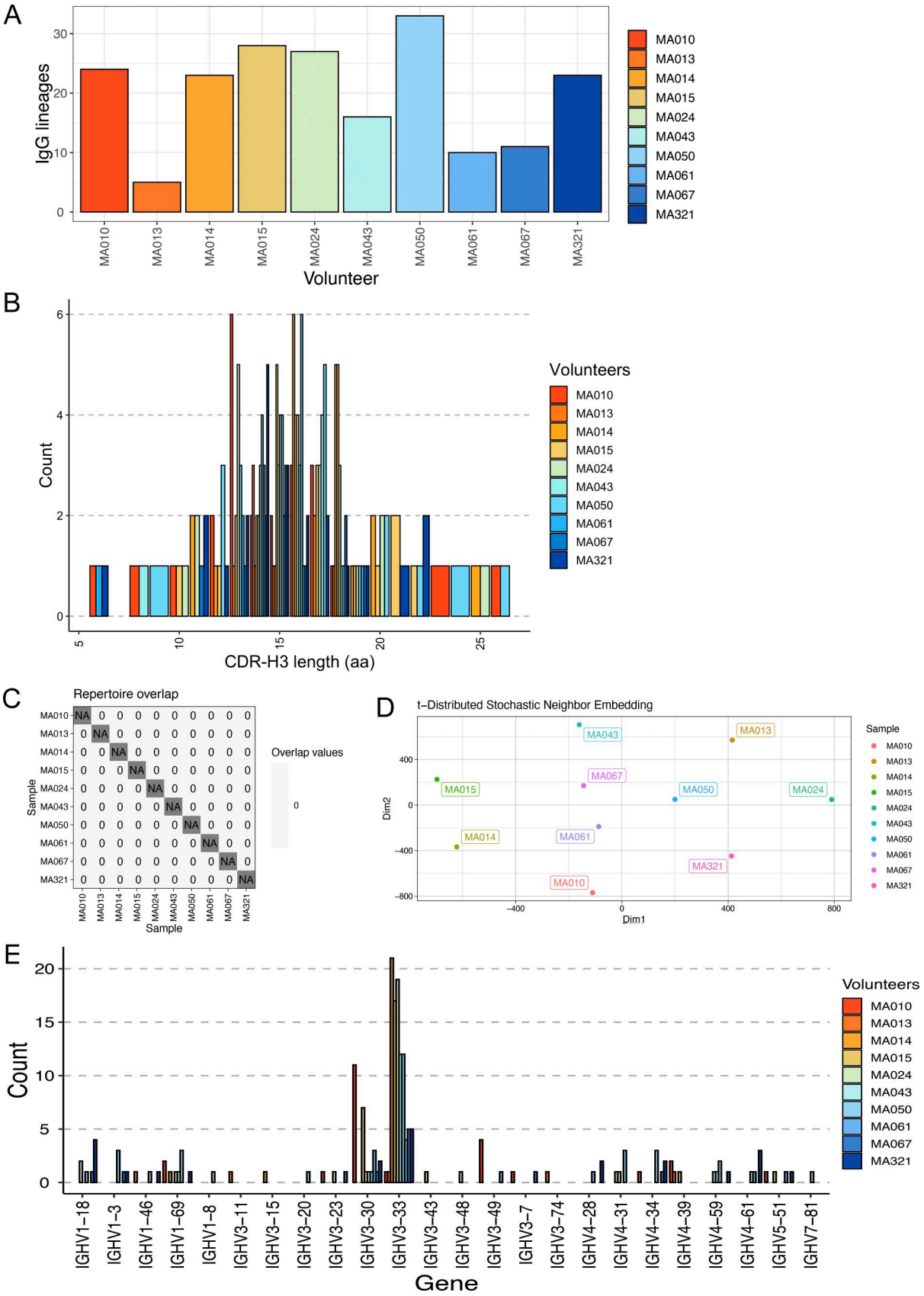

Figure S1. **Profile of NANP$_6$-reactive IgG repertoires across all 10 volunteers after vaccination. (A)** Number of IgG lineages per volunteer. **(B)** Frequency of CDR-H3 lengths for all lineages. **(C)** Checkerboard graphic illustrating no shared CDR-H3s (no overlap) across volunteers. **(D)** Dissimilarity of VH repertoires according to tSNE analysis. **(E)** Frequency of IGHV gene use by volunteer.

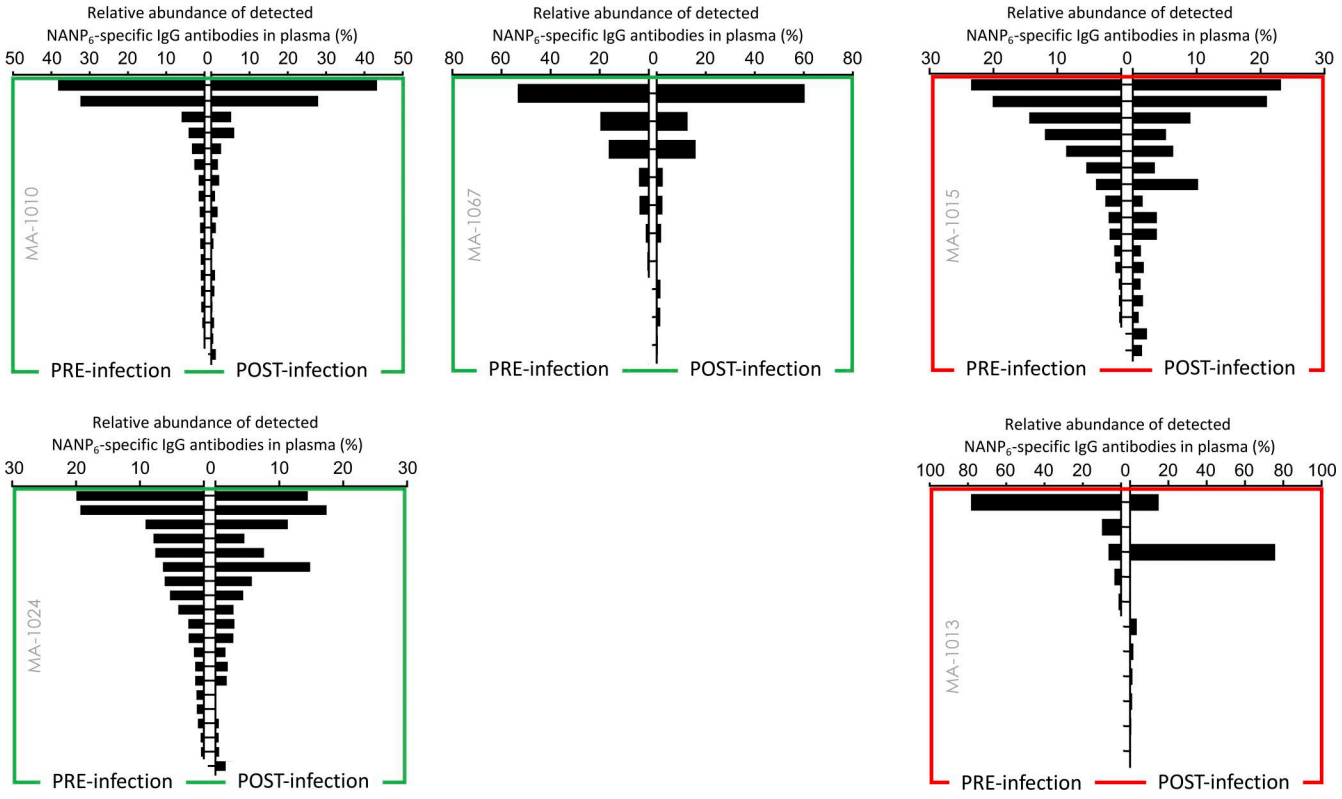

Figure S2. **Static composition and high correlation between $NANP_6$ pre-challenge and post-challenge IgG repertoires among VAC065 volunteers.** A green outline indicates the volunteer was protected from infection; red indicates they were not protected.

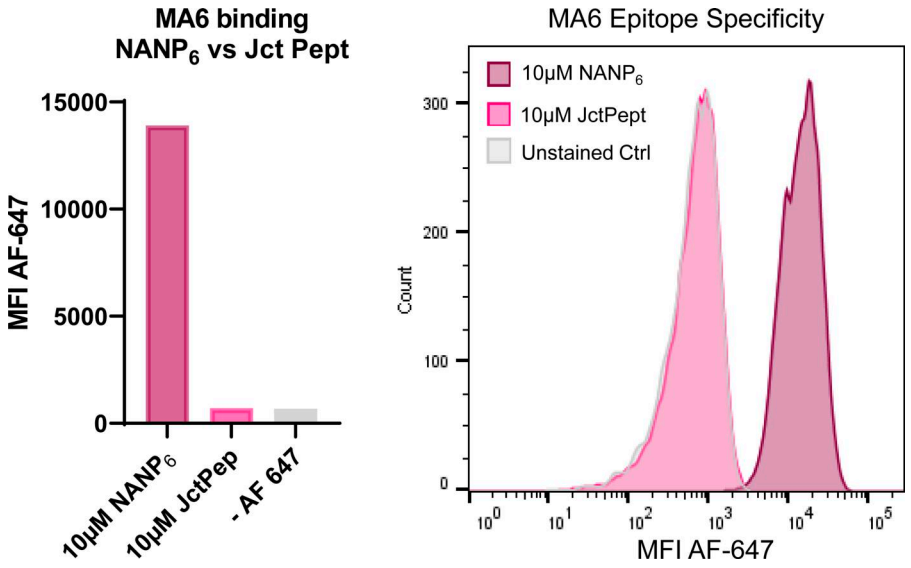

Figure S3. **MA6 epitope specificity.** MA6 Fab fragments displaying yeast were incubated with 10 μM biotinylated $NANP_6$ or JR peptide (Jct Pept: KQPADGNPDPNANPNVDPN) and subsequently labeled with streptavidin-conjugated Alexa-Fluor 647 to detect binding via flow cytometry.

Provided online is Table S1. Table S1 shows the R21 Ig-Seq repertoire summaries for each subject.